# EFFECT OF ZINC SUBSTITUTION ON THE STRUCTURE OF CALCIUM FLUORO-ALUMINO-SILICATE GLASSES AND GLASS-CERAMICS


**By**

**Siqi Zhang**

A thesis submitted to the School of Metallurgy and Materials of University of Birmingham for the degree of

**MPhil**

School of Metallurgy and Materials
The University of Birmingham

**October 2010**

## TABLE OF CONTENTS

## ABSTRACT

Ionomer glasses are certain glass compositions that have been used as the glass component in glass ionomer cements. The term “ionomer” was traditionally related with the use of polyacrylic acid as the polymeric component of glass ionomer cements that incorrectly was characterized as an ionomer polymer. The name has been retained and therefore the glass compositions used in these materials are called ionomer glasses. A typical ionomer glass molar composition is $4.5SiO_2$-$3Al_2O_3$-$1.5P_2O_5$-3CaO-$2CaF_2$. The glass can be made by a melt-quench route at 1450˚C. This glass composition has been extensively studied. Substitution of other divalent cations for calcium can offer a range of different properties in the glass including radiopacity. Sr, Ba and Mg substitutions lead to the conclusion that the cation size plays a very important role on the microstructure of the amorphous glass and the glass ceramic. This work focuses on zinc substitution for calcium. Zinc compared to calcium is a smaller cation with an atomic radius of 1.34 Å against 1.97 Å for calcium. Zinc has been proven to be bactericidal and has shown ability to stimulate osteogenesis. A series of zinc substituted glasses were produced by replacing Zn for Ca in 25mol% (LG26 25%Zn), 60mol% (LG26 60%Zn), 75mol% (LG26 75%Zn) and 100mol% (LG26 100%Zn). The new glasses were characterized by Helium Pycnometer, DSC, TGA, FTIR, Raman, ESEM and EDX. The density of the resulting glass ceramics was measured also by Helium pycnometer and X-ray diffraction was conducted to identify the crystal phases formed.

The density of zinc substituted glasses and glass-ceramics increased with increasing the zinc content. However, the oxygen density did not change significantly indicating a rather stable network that was not affected by zinc substitution. The glass transition temperature decreased with zinc substitution whereas the crystallization temperature was affected by the particle size of the glasses and although when coarse particles

were studied crystallization was not recorded, when fine particles were studied the crystallization temperature generally increased with substitution and above 60% of substitution only one crystallization temperature was recorded. Isothermal studies for the coarse glass particles were conducted in order to study the crystallization process that was believed to be very slow. The crystallization temperatures recorded had an increasing tendency with zinc substitution. An endothermic transition appeared at a relatively low temperature (ca 1200$^{o}$C) was interpreted as a crystal dissolution temperature that decreased with zinc substitution. FTIR and Raman spectroscopy showed an increase in bridging oxygens with zinc substitution. The crystallized materials exhibited sharper and more distinct peaks that corresponded to new bond formation due to different crystal phases formed. While the calcium base glass composition crystallized to Fluorapatite and mullite, zinc substitution led to the formation to a gahnite ($ZnAl_2O_4$) and calcium zinc phosphate ($CaZn_2(PO_4)_2$) phases. ESEM and EDX analysis showed changes in the morphology of glass ceramics with zinc substitution.

## ACKNOWLEDGEMENTS

I am so grateful to my academic supervisor, Artemis Stamboulis, for her presence, encouragement, support and guidance throughout the year.

I would like to thank XiaoHui Chen from Queen Mary University of London helping me to make the zinc substituted glasses, and James Bowen from our university chemical engineering helping me to do the Raman analysis, Georgia Kaklamani and Zahira Jaffer from our biomaterial group for being always present and willing to provide assistance during my research and they overall support,.

I would also like to thank Paul, Jess, and Frank for teaching me how to use the DSC, TGA, FTIR, XRD, ESEM and EDX machines and the many kindnesses they show me.

Finally, I would like to thank my family, for believing in me and supporting me and always being next to me in every step I choose to take.

## FIGURE CAPTIONS

## TABLE CAPTIONS

## ABBREVIATIONS

| | |
|---|---|
| **BO** | **Bridging Oxygen** |
| **DSC** | **Differential Scanning Calorimetry** |
| **EDX** | **Energy dispersive X-ray analysis** |
| **ESEM** | **Environmental scanning electron microscope** |
| **FAP** | **Fluorapatite** |
| **FTIR** | **Fourier Transform Infra-Red Spectroscopy** |
| **GICs** | **Glass ionomer cements** |
| **GPCs** | **Glass polyalkenoate cements** |
| **NBO** | **Non-bridging oxygen** |
| **PAA** | **Polyacrylic acid** |
| **SEM** | **Scanning electron microscope** |
| **TGA** | **Thermogravimetric analysis** |
| **XRD** | **X-ray powder diffraction** |

# CHAPTER 1: INTRODUCTION

## 1.1 Introduction

Calcium fluoro-alumino-silicate glasses which are commonly used for the formation of polyalkenoate cements have significant applications in the medical and dental fields. Previous studies have shown that such glasses can crystallize to form fluorapatite [1-2]. Many interests have gained on fluorapatite glass-ceramics since apatite is an important mineral phase of tooth and bone. However, the effects of Zn addition on apatite-forming ability and its biocompatibility on glass-based materials have not been reported.

This study will focus on the effects of zinc substitution over calcium to produce substituted alumino-silicate glasses and glass ceramics. The cation substitution takes place in 25%, 60%, 75% and 100% molar content of zinc. The samples are all characterised by DSC, TGA, FTIR, RAMAN, XRD, ESEM, EDX and MAS-NMR in order to observe the effect of zinc substitution on the structure of glasses and glass-ceramics.

## 1.2 Literature Review

Glass ionomer cements (GICs) or glass polyalkenoate (GPCs) formed as a result of the reaction between an aqueous solution of polyacrylic acid (PAA) and a powder of a fluora-alumino-silicate glass, have been extensively applied as restorative, cavity liners and bases in dentistry since their development by Wilson and Kent in1969 in the Laboratory of the Government Chemist in UK [3-6]. The first commercial dental

cements had considerably inferior properties compared to the materials today [7, 8], which were released to the market in 1975. The glasses for incorporation into GICs are commonly called “ionomer glasses” and are in general composed of 20-36 wt% $SiO_2$, 15-40% $Al_2O_3$, 0-35% CaO, 0-10% $AlPO_4$, 0-40%$CaF_2$, 0-5% $Na_3AlF_6$ and 0-6%$AlF_3$ [9]. When the acid attacks the glass structure in the setting reaction, cations are released into the aqueous phase that subsequently cross-link the PAA chains, resulting in the production of a cement with a hydrated polysalt matrix in which the glass particles are embedded [10, 11]. The most important characteristic of ionomer glasses is the presence of a large quantity if fluorine that leads to a lower refractive index of the glass resulting in an improved translucency of the cement. In addition, the long-term fluoride release inhibits the formation of secondary caries, whereas the compressive strength is enhanced and reaches values above 200 MPa [12, 13]. In the past ten years, there has been substantial development of ionomer glasses. For example, the new glass systems do not usually lose very small amount of fluorine during melting in the form of $SiF_4$ compared to the earlier glass systems [14-17]. It has been reported, that the composition and structure of glasses have strong influence on the subsequent cement properties, like viscosity, fracture toughness, compressive strength, Young’s modulus, and so on [10 , 18, 19]. In addition, glasses with appropriate compositions can be heat-treated and thus undergo controlled crystallization to form glass-ceramics, in which the main crystalline phase is apatite and similar to the apatite phase in bones and teeth [20-23].

During the past 50 years, advances in many specialty bioceramics such as alumina, zirconia, hydroxyapatite, tricalcium phosphates and bioactive glasses have made significant contribution to the development of modern health care industry and have improved the quality of human life. These ceramics are primarily used as bone substitutes in the biomedical industry due to their biocompatibility, low density, chemical stability, high wear resistance, and for calcium phosphates, mainly for their compositional similarity with the mineral phase of bone. The main constituents of

bone are collagen 20wt%, calcium phosphate 69wt%, and water 9wt% [24].

Monroe et al. and Levitt et al. were the first people to suggest that calcium phosphate ceramics are appropriate for use as dental and medical implant materials. Calcium phosphate glasses are well-known for their biocompatibility and bioactivity for bone healing applications [25]. Ducheyne et al. have demonstrated that calcium phosphate ceramics have the ability to bond with bone and thus promote bone formation [26]. Calcium phosphate glasses have numerous of other applications, for instance, use as immediate tooth root replacement, restores metal implants, coating for metal implants and use as bone filling for the repair of periodontal defects. Despite of their similar composition as compared to the bone, the brittleness of calcium phosphate glasses always hinders its application as bone cements. Thus, calcium phosphate glasses are mainly used as coatings instead [27]. Apatite-mullite glass ceramics, on the other hand have been developed with the view to be used in bone repair due to the high fracture toughness values reported in the literature [28].

**Glass compositions and design roles**

A large number of ionomer glass compositions have been studied as cement formers until now and among them three major categories of glasses can be identified:

(1) Aluminoborate glasses: The glasses are based on the general composition $Al_2O_3$-$B_2O_3$ with addition of $Na_2O$, $Li_2O$, BaO, ZnO, $ZnF_2$ etc [29-34]. Aluminoborate glasses are of interest, due to their instability in hydrolysis after proper heat treatment leading to controlled reactivity of the glass ionomer cements and also due to their high electrical resistivity, which is higher than that of silica [30, 35]. However, the relatively poor chemical durability of the aluminoborate glasses as well as the low compressive strength of the corresponded cements compared to the aluminosilicate glass formed ionomer cements have restrained the use of aluminoborate glasses in dental applications [36, 37]. Besides, the increasing B2O3 addition raises the dissolution rate of borosilicate glasses and therefore $B_2O_3$ cannot

be used in high amounts in the glass composition [38].

(2) Aluminosilicate glasses: the glasses are based on the general composition of $SiO_2$-$Al_2O_3$-CaO or $SiO_2$-$Al_2O_3$-$CaF_2$, and have been studied mostly by Wilson and co-workers [39]. Recently, individual compositional ingredients have been changed by different researchers, and many of the present glasses are made of $SiO_2$, $Al_2O_3$, CaO, $CaF_2$, NaF, $K_2O$ and $P_2O_5$ [40, 41]. Today, all the commercial glass compositions used for cements formation are alumino-silicate glasses with additional calcium and fluorine ions. Alumino-silicate glasses are some of the oldest known glasses but are also one of the least understood materials for their structure and chemical bonding. In addition, they are used for their chemical durability, tolerance in higher temperatures and superior strength properties as glass ceramics [42-44].

(3) Zinc silicate glasses: The glasses are based on the general compositions CaO-ZnO-$SiO_2$ or $Al_2O_3$-ZnO-$SiO_2$ [45-47]. In the CaO-ZnO-$SiO_2$ ternary system, zinc acts as both a network modifier and an intermediate oxide like alumina as reported by R.Hill et al. [45]. In addition, the release of zinc enhances bone formation and mineralization by directly activating the aminoacyl-tRNA synthetase in osteoblastic cells as well as stimulating cellular protein synthesis [46]. Moreover, zinc is important for the function of the immune system and has been recognized as an antibacterial agent [47, 48]. There is a high percentage of zinc oxide and silica in both CaO-ZnO-$SiO_2$ and $Al_2O_3$-ZnO-$SiO_2$ glass compositions with only a little amount of the third oxide. All of the above advantages give zinc silicate glasses a great potential as cement formers and hard tissue replacement materials. Despite the advantages reports suggest [16, 49], that the zinc glass based cements have inferior mechanical properties compared to the corresponding aluminosilicate glass based cements for use in clinical dentistry. Thus, zinc silicate glasses are believed to have great potential as cements formers and hard tissue replacement materials.

Recently, zinc was incorporated into the Ca-Si system, forming a material referred as Hardystonite ($Ca_2ZnSi_2O_7$), which possesses improved mechanical properties with

increased bending strength and fracture toughness as compared to hydroxyapatite (HAP) [50]. Zinc cation ($Zn^{2+}$) has been found to be osteoconductive stimulating osteogenesis. A simply blended mixture of ZnO/hydroxyapatite was also used to form a bone cement with polyacrylic acid aqueous solution that exhibited low compression stress (<100MPa) and working time of less than 1 minute and therefore it was less attractive for orthopaedic applications [51, 52].

Due to the properties of glass and glass-ceramics being determined critically by their composition, the crystallization process and the microstructure, both the design and characterization of these glasses play very important role in the development of new medical glasses.

Many models have been used to interpret the glass structure, however all models are based on the Zachariasen's random network theory. In fact, the term 'random network' never appeared in Zachariasen's classic paper, which was mainly written as an explanation for glass formation tendency at that time. Zachariasen [53] stated that the atomic forces and internal energy must be of the same order in both the glasses and the related crystals, in addition, the internal energy difference between the glasses and the corresponding crystal must be very small requiring an open and flexible structure. Therefore, Zachariasen defined a glass as "a substance that can form an extended three-dimensional network that is lacking periodicity with energy content comparable with that of the corresponding crystal network". Finally, Zachariasen summarized four rules for glass formation, which have been developed during extensive usage and practical observations into a set of rules for formulating a continuous 3-dimensional glass network and are summarized below [6]:

(1) Each oxygen atom is linked to no more than two cations.
(2) The oxygen coordination number of the network cation is small.
(3) Oxygen polyhedra share only corners and not edges or faces.
(4) At least three corners of each oxygen polyhedron must be shared in order to form a 3D network.

(5) The glasses must contain a high percentage of network cations which are surrounded by oxygen tetrahedral.
(6) The oxygen tetrahedral share only corners with each other.
(7) Some oxygens are linked only to two network cations and do not form further bonds with any other cation.

Zachariasen suggested that sharing corners is a crucial condition in order to get a random structure. In this model therefore, assemblies of only individual $[SiO_4]^+$ tetrahedral are connected at the corners to form chains in the simplest possible glass network, which would be opposed to acid attack linked with its electro neutrality. But this behaviour of glass can be changed with the introduction of aluminium by providing negative charge in the glass structure. In accordance with Lowenstein's rule [54], aluminium in four-fold coordination can substitute for silicon in the tetrahedral $[AlO_4]^{5-}$ and break the electron balance by leaving a negative surplus charge in each tetrahedron. Positively charge ions like $Ca^{2+}$, $Na^+$, $Mg^{2+}$ or $Al^{3+}$ will compensate the negative charge serving as glass network modifiers. There is a ratio limit for Al/Si, which must be smaller or equal to 1, because above this value aluminium would not be able to adopt the tetrahedral linked by one oxygen bridge, the centre of only one of them can be occupied by aluminium, whereas the other centre must be occupied by silicon or another small ion of four or more electrovalence, like phosphorus. Similarly, whenever two aluminium ions are neighbours to the same oxygen anion at least one of them must have a coordination number higher than four, e.g. five or six, towards oxygen. All oxygen in the glass structure is bridging oxygen (BO), and the non-bridging oxygen (NBO) can be formed by including other species such as CaO and $Na_2O$ in the glass composition. It has been reported, that in simple aluminosilicate glasses transformation of BO to NBO can take place [55]. A schematic diagram is shown in Figure 1.1. Due to this effect of CaO on the glass structure, calcium is defined as a glass network modifier. Aluminum can also function as an independent cation with a coordination number of five or six towards oxygen, with the exception of replacing silicon and taking up a four-fold coordination to form aluminum

tetrahedral.

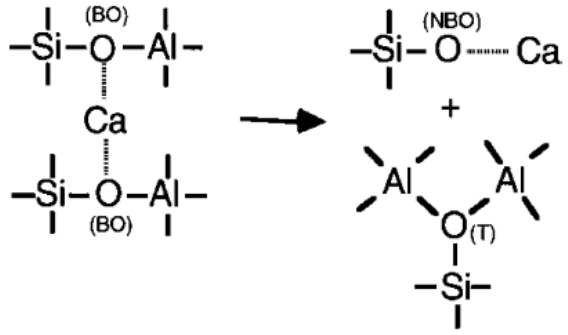


**Figure 1.1**: Schematic diagram of bridging oxygen (BO) to non-bridging oxygen (NBO) transformation according to Stebbins and Xu 1997 [55].

**Glass Structure**

A lot of effort has been executed in understanding glass structure with the aim to gain deep insight into the relationship between structure and properties (thermodynamic and mechanical). This knowledge can be exploited for the design of new materials [19, 30, 45]. Calcium fluoro-alumino-silicate glasses are widely used to form glass ionomer cements for medical and dental applications, and are able to crystallize into an apatite and mullite phase and form apatite-mullite glass-ceramics, that have shown excellent osteointegration and osteo-conduction properties when implanted in the body as has been reported by Freeman et al. [56]. Among other aluminosilicate glasses, the glass system based on the general composition $SiO_2$-$Al_2O_3$-$P_2O_5$-CaO-$CaF_2$ has been extensively studied [9, 15, 20, 57-62]. Factors such as the alkali content, the Al/Si ratio, the fluorine and phosphorus content has been shown to have an effect not only on the glass properties but also on the properties of the resulting glass-ionomer cements and glass ceramics [16, 18].

Previous studies showed that the aluminium to silicon ratio can be a dominant factor, affecting the reactivity of glasses with simple composition CaO-$Al_2O_3$-$SiO_2$ and also the properties of the corresponding glass ionomer cements [18, 39]. However, Griffin et al [16] suggested that the ratio of Al/Si is much less important in more complicated

glass compositions containing phosphorus and fluorine, and has barely any significant influence on the cements properties. Most of silicon and aluminium tetrahedral are polymerized to form bridging oxygen (BO) sites Si-O-Si, Si-O-Al and Al-O-Al with small amount of non-bridging oxygens (NBO) in charge balanced aluminosilicate glasses [55]. The acid degradability of alumino-silicate glasses is related to the destabilization of the coordination state of aluminum due to the exchange of charge balancing cations connected with the charge deficient $AlO_4$ tetrahedral [54]. Kirkpatrick et al. suggested that phosphorus may occupy the neighboring tetrahedral sites to $AlO_4$ tetrahedral with $P^{5+}$ ion charge balancing the charge deficient $Al^{3+}$ ions [63, 64] and therefore the numbers of Al-O-Si species available for acid hydrolysis are reduced. The ratio of aluminium to phosphorus can also have an effect on the number, type and rate of ion release from the glass [17]. In addition, alkali metal ions like sodium are added to ionomer glasses with the intention to decrease the melting temperature during glass production and to help the release of fluoride ion with offering a soluble counter ion [8].

A lot of interest has been shown on the structural role of fluorine in ionomer glasses [65, 66]. The fluorine content serves two major roles in glass: Firstly fluorine decreases the melting temperature and the viscosity and secondly it disrupts the glass network facilitating the acid attack during cement formation [63]. As a network disruptor, the addition of calcium fluoride may lead to the formation of non-bridging fluorines as well as non-bridging oxygens illustrated in Figure 1.2 [18]. While calcium modifies the glass network charge balancing NBO's and the charge deficient $AlO_4$ tetrahedra [18]. Fluorine replaces BO's with non-bridging fluorines. Glasses based on the generic composition $4.5SiO_2$-$3.0Al_2O_3$-$1.5P_2O_5$-$(5.0\text{-}x)CaO$-$xCaF_2$ with X varying from 1 to 3.0 have been investigate by Griffin and Hill [14], in order to study the influence of fluorine on glass properties. Introducing fluorine to the glass structure, a decrease of 200'C in the glass transition temperature can be observed. This is expected as the glass network connectivity is reduced by fluorine replacing bridging oxygens with non-bridging fluorines, allowing the network relaxation to

occur at a lower temperature.

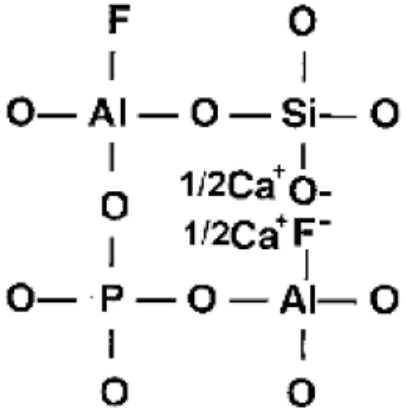


**Figure 1.2**: Schematic illustration showing the structural role of calcium and fluorine in ionomer glasses [18].

A study on the coordination environment of fluorine in the glass network can give a clear understanding of the mechanism by which glass properties can be affected. Recently, a number of MAS-NMR studies on the structure of aluminosilicate glasses have contributed profoundly to the above. Hill and Wood [15] studied a series of glasses based on the composition of $2SiO_2$-$Al_2O_3$-$2(1-x)CaO$-$xCaF_2$, and reported, that fluorine is bonded to aluminum atoms instead of silicon atoms. However, earlier studies by Wilson et al. [39, 67] on a series of glasses based on $xSiO_2$-$yAl_2O_3$-$zCaF_2$ suggested, that fluorine formed Si-F and Al-F bonds in $SiO_3F$ and $AlO_3F$ tetrahedral, respectively and thus it was suggested, that fluorine disrupted the glass network by substituting bridging oxygens with non-bridging fluorines as fluorine cannot bridge $SiO_4$ tetrahedra. Zeng et al. [68] confirmed, that considerable fractions of network Al-O bonds are replaced by weaker non-network Al-F bonds, and suggested that the formation of non-network Si-F bonds can be significant in aluminosilicate glasses given that Si-F-Ca (n) species occur in the range of 123.4 to 134.5ppm. It is possible, The formation of Si-F bonds connected with the glass composition in addition to the fluorine content. Stebbins and Zeng [69] found evidence for the presence of Al-F-Ca (n) and F-Ca (n) species in the glass network, where n represents the number of Ca next nearest neighbouring fluorine in a $2SiO_2$-$2Al_2O_3$-$0.5CaF_2$ glass.

## Crystallization of glasses

An important advantage of the ionomer glasses described above is that they can crystallize into apatite containing glass-ceramics, which are under wide investigation for restoring and replacing hard tissues in the orthopaedic and dental fields as the apatite phase is similar to the biological apatite in teeth and bones [44, 70]. A large quantity of research has been dedicated to the development of hydroxyapatite (HA) based materials formed by a sintering route, which however, encounters the following problems: i) degradation of sintered HA at high temperatures, ii) insufficient strength and toughness of sintered materials, and iii) subsequent machining is required using diamond-tipped tools to cut the desired shapes that is normally an expensive, difficult and time consuming process. Compared to sintering and machining, the thermal annealing process of cast shaped glasses in order to make glass-ceramics is a desirable production route for making apatite based materials. In this case machining of the glass ceramics is not required. In the past two decades, various glass ceramics have been developed and categorized generally into three different groups: (1) the apatite-wollastonite glass-ceramics developed by Kokubo et al. [71] based on a glass composition of $SiO_2$-$P_2O_5$-CaO-MgO, (2) the mica based materials originally developed by Grossman [72], including the commercially available DicorTM for producing dental crowns and (3) the apatite-mullite glass-ceramics developed by Hill et al. [20, 59]. Apatite is the primary phase in both the apatite-wollastonite and apatite-mullite systems, moreover, which is in accordance particularly with fluorapatite on the apatite-mullite system. Fluorapatite has higher stability than the hydroxyapatite mineral phase, given that the fluoride ion is smaller than the hydroxyl ion and packs more readily into the apatite crystal lattice. Furthermore, the resulting fluoride release and its cariostatic effect make the apatite-mullite system more attractive to the growing application of tooth saving preparation methods, such as tunnel techniques. Therefore, for the purpose of this work great emphasis will be put on the crystallization of castable apatite-mullite glass-ceramics based on the general

composition of $4.5SiO_2$-$3Al_2O_3$-$1.5P_2O_5$-(5-x) CaO-x$CaF_2$, where x is between 0 and 3.

The high fluorine containing glasses has been found by Rafferty et al. [73] that could crystallize to fluorapatite (FAP, $Ca_5(PO_4)$) and mullite ($3Al_2O_32SiO_2$) during the heating process which was accompanied by a decrease in crystallization temperatures with increasing $CaF_2$ content. ß-$Ca_3(PO_4)_2$ (ß-tricalcium phosphate) and $CaAl_2Si_2O_8$ (anorthite) were the two crystalline phases formed in the fluorine free glass ceramics. It was therefore suggested, that the fluorine may have a remarkable influence on the nucleation and crystallization behaviour of these glasses. The crystallized glass ceramics exhibited high fracture toughness and high strength (260MPa) [43], which can be explained by the FAP-mullite interlocking structure obtained after bulk nucleation via prior amorphous phase separation (Figure 1.3).

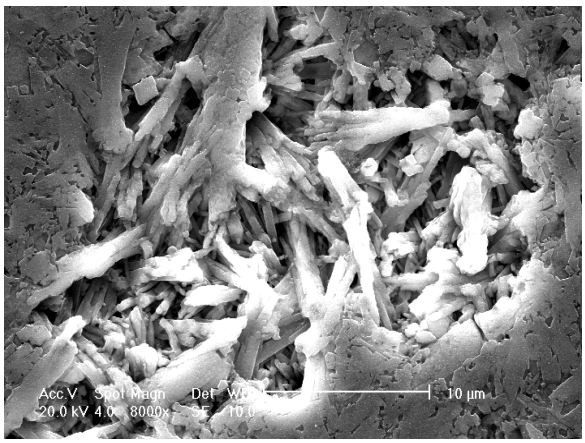


**Figure 1.3**: ESEM of an apatite - mullite glass-ceramic of the composition $4.5SiO_2$-$3Al_2O_3$-$1.5P_2O_5$-3CaO-2$CaF_2$ (LG26 100%Ca) heat treated to the second crystallization temperature exhibiting an interlocking microstructure.

The crystallization of glasses is attributed to thermodynamic drives for reducing the Gibbs' free energy, and the amorphous phase separation (APS) or glass-in-glass phase separation favours the crystallization process by forming a nucleated phase easier than it would be formed in the original glass. In fact, the glass microstructure at a few hundred atoms scale is not as homogeneous as a perfect single crystal or a liquid

solution, although it appears often homogeneous. There are two routes resulting in the formation of inhomogeneous glass microstructure, the following: 1) by the crystallization or devitrification, where definite crystals nucleate and grow from a super cooled liquid mass; or 2) by applying the Lebedev crystallites theory to understand the microstructure, that is the crystallites are not microcrystal but they possess distorted lattices and have definite chemical composition that is determined by the phase equilibrium diagram of the glass composition. The glass can be considered simply as a liquid that undergoes demixing process when it cools. If both of these two phases are liquids, then the phase separation is called liquid-liquid immiscibility. The immiscibility is defined as stable or metastable, which is up to whether the phase separation occurs at temperatures above the liquidus or below the liquidus. The latter case is more absorbing, by which there are two processes causing the formation of discrete phases: the nucleation and growth mechanism [74-76] and spinodal decomposition [75, 77]. For the duration of spinodal decomposition, both phase compositions change with time until equilibrium is reached, and the interface between phases is diffusing and eventually sharpens. The second phase tends to produce non-spherical particles with high connectivity and is distributed regularly in both size and position. On the other hand during nucleation and growth, the second phase does not change its composition at a constant temperature with time but there is always a sharpening interface formed between phases during growth. The second phase consists of spherical particles with very low connectivity, the particle size and position of which are randomly distributed.

**Aims and Objectives**

In the present study, addition of zinc oxide to the above ionomer glass composition is expected to have an effect on the structure of the glass as well as the formed glass-ceramics. Consequently it is also expected that the produced glass ceramics might have stimulatory effects on bone formation. However, more importantly if Zn would act as an intermediate oxide, this will allow the design of new aluminium free

glass compositions for bioceramics applications as well as dental and bone cements.

The purpose of the present work is to study the influence of zinc substitution on the structure of fluorine containing calcium-alumino-silicate glasses and the resulting glass-ceramics. All the substituted glasses are based on the composition of $4.5SiO_2$-$3Al_2O_3$-$1.5P_2O_5$-3CaO-$2CaF_2$, which can crystallize to fluorapatite (FAP) and mullite on appropriate heat treatments. The main objectives of this research are:

1. To produce fluorine containing calcium-alumino-silicate glasses and to develop substituted zinc glass compositions.
2. To investigate the effect of zinc on the microstructure of glasses and glass-ceramics.
3. To study the crystallization process and determine the crystalline phases.

# CHAPTER 2: METHODS AND MATERIALS

## 2.1 Ca-alumino Silicate Glass

The glass with composition $4.5SiO_2$-$3Al_2O_3$-$1.5P_2O_5$-$3CaO$-$2CaF_2$ which has an excess of fluorine content compared to the FAP stoichiometry Ca : P : F = 5 : 3 :1 was selected for this study. Lowenstein's rule demands that, whenever two tetrahedral are linked by one oxygen bridge, the center of only one of them can be occupied by aluminum; the other center must be occupied by silicon, or another small ion of electrovalence of four or more, e.g. phosphorus [54]. According to Lowenstein's rules, this glass contains sufficient phosphorus and silicon to allow the aluminum to take up a four-fold coordination state. The selected glass composition is in accordance with other glass criteria which include: a) the presence of at least one NBO for each silicon and b) the amount of fluorine in the glass should be less than that of aluminum in order to minimize the formation of volatile $SiF_4$ during melting [59]. The second criterion can be explained on the basis that one $Si^{4+}$ cation can be involved easier with NBOs or $O^{2-}$ anions than with a non-bridging fluorine or $F^-$ anion and that an $Al^{3+}$ ion should bond to $F^-$ anions preventing the formation of Si-F bonds in the glass network. The explanation is supported by a trimethylsilylation analysis reported in a previous study of $2SiO_2$-$Al_2O_3$-$CaO$-$CaF_2$ glass that showed absence of Si-F bonds in the glass structure [15].

## 2.2 Preparation of Calcium fluoro-alumino-silicate glasses with Zn substitution

The molar composition of the fluorine containing alumino-silicate glasses is shown below in Table 2.1.

**Table 2.1**: Molar composition of Zn substituted alumino-silicate glasses

| Glass code | $SiO_2$ | $Al_2O_3$ | $P_2O_5$ | CaO | $CaF_2$ | ZnO | $ZnF_2$ |
|---|---|---|---|---|---|---|---|
| LG26Ca(100%) | 4.5 | 3 | 1.5 | 3 | 2 | 0 | 0 |
| LG26Zn(25%) | 4.5 | 3 | 1.5 | 1.75 | 2 | 1.25 | 0 |
| LG26Zn(60%) | 4.5 | 3 | 1.5 | 0 | 2 | 3 | 0 |
| LG26Zn(75%) | 4.5 | 3 | 1.5 | 0 | 1.25 | 3 | 0.75 |
| LG26Zn(100%) | 4.5 | 3 | 1.5 | 0 | 0 | 3 | 2 |

The glass components silicate dioxide ($SiO_2$), aluminium oxide ($Al_2O_3$), phosphorus pentoxide ($P_2O_5$), calcium fluoride ($CaF_2$), zinc oxide (ZnO), zinc fluoride ($ZnF_2$) and calcium carbonate ($CaCO_3$), which will provide calcium oxide (CaO), were weighed out in order to receive approximately 100 g of glass for each composition. The powders were mixed by hand for 30 min and the resulting mixture was transferred in a platinum rhodium (Pt, 5% Rh) crucible. The crucible was then placed in an electric furnace (EHF 17/3, Lenton, UK) for a period of 1.5 hours at a temperature of 1450°C. After this period, the glass melt was poured into deionized water to prevent phase separation and crystallization resulting in frit glass, in the case of 25%Zn glass the frit was ground with the help of a pestle and mortar and sieved to give fine particles (<45μm) and coarse particles (45μm-100μm). The 60% and 75%Zn glasses were milled in a gyro mill for 14 minutes and was subsequently sieved to give fine particles (<45μm) and coarse particles(45μm-100μm) for further analysis.

The LG26 100%Zn glass composition was crystallized during glass making and therefore this composition will not be discussed in the thesis.

## 2.3 Differential Scanning Calorimetry (DSC)

Differential scanning calorimetry was used in order to examine the thermal transitions in glasses. The information obtained by this method is the values for the glass transition temperature ($T_g$), peak crystallization temperature ($T_p$) and melting point ($T_m$). The instrument used was a NETZSCH 404C DSC with pairs of matched platinum-rhodium crucibles, and all the runs were performed on 20 mg samples in dry argon at a heating rate of 10$^o$C/min. The analysis was a direct comparison among the DSC curves of glasses of different particle size in order to determine their tendency to undergo either surface or bulk nucleation. This analysis is based on the principle that the surface area per unit volume of glass increases with decreasing the particle size providing a greater chance for the surface nucleation to occur if the glass is prone to surface nucleation. A distinct sharp crystallization peak will normally appear with decreasing the particle size if the glass under assessment nucleates and crystallizes on the surface. Furthermore, the crystallization peak temperature should move to lower values with decreasing the particle size.

## 2.4 Crystallization of glasses

Fine particles of glasses were weighed out (approximately 2g) and poured in a die in order to form homogeneous tablets which then were placed in a platinum crucible for further heat treatment. The crucible was placed in an electric furnace and the heating rate was 10°C/min. When the furnace which was used EHF 17/3 (Lenton, UK) reached the $T_{p2}$+50$^o$C, the sample was held for 1 hour for crystallization to complete. Afterwards, the furnace was switched off and the temperature was decreased to room temperature.

## 2.5 Helium Pycnometer – Density Measurements

The density of glasses and glass ceramics was measured using the method of helium pycnometer. Gas pycnometry is a common analytical technique that uses a gas displacement method to measure volume accurately. Inert gas, such as helium is used as the displacement medium. The sample is sealed in the instrument compartment of known volume, the appropriate inert gas is admitted, and then expanded into another precision internal volume. The pressure was measured before and after expansion and is used to calculate the sample volume. Dividing this volume into the sample weight gives the gas displacement density.

The AccuPyc II 1340 Series Pycnometer was used for density measurements of glasses and glass ceramics is automatic and provides density calculations on a wide variety of powders, solids, and slurries having volumes from 0.01 to 350 $cm^3$. In our case the samples were <45μm of particle size and their mass was approximately 1gr. The instrument completed sample analyses in thirty minutes providing us with 10 consecutive measurements as well as the deviation of each measurement. In order to calculate the density of the glasses and glass ceramics we took the average of these ten consecutive measurements.

The oxygen density was calculated in order to provide us with an indication of the change of network connectivity with substitution.

Then the oxygen density of glasses was calculated by using the following equation 2.2:

$$Oxygen\ Density = \ Density\ \times \frac{molecular\ weight\ of\ oxygen}{molecular\ weight\ of\ glass} \qquad \text{(Eq 2.2)}$$

## 2.6 Fourier Transform Infra-Red Spectroscopy (FTIR) and Raman Spectroscopy

Fourier Transform Infra-Red Spectroscopy (FTIR) is a technique with which information about the chemical structure of a material can be obtained by using a Perkin-Elmer FTIR spectrometer (Spectrum2000, Perkin Elmer, USA). When infrared radiation is absorbed by a material, the chemical bonds of the material begin to vibrate. Functional groups tend to absorb infrared radiation at a specific wavenumber region. This region is independent of the structure of the molecule that the functional group may belong to. Consequently, it is obvious that the wavenumbers and the chemical structure are related, thus an unknown molecule can be identified by its FTIR spectra [78, 79].

In order to get the spectra, a ratio of 1:100 of the sample and potassium bromide (KBr) were used. The KBr was used in order to increase the resolution of the spectra obtained. The background using a control sample of KBr was always taken prior to each measurement. The Diffuse Reflectance Accessory was used so as to get a spectrum of 4000-400 nm. The resolution was 4 $cm^{-1}$ and the number of scans was 100 per minute.

Raman spectroscopy is a spectroscopic technique used to study vibrational, rotational, and other low-frequency modes in a system [80]. It relies on inelastic scattering, or Raman scattering, of monochromatic light, usually from a laser in the visible, near infrared, or near ultraviolet range. The laser light interacts with molecular vibrations, phonons or other excitations in the system, resulting in the energy of the laser photons being shifted up or down. The shift in energy gives information about the phonon modes in the system.

Raman spectroscopy is concerned primarily with the vibrational energy level transitions of molecules. By monitoring the inelastically scattered photons we can

probe molecular vibrations, and the Raman spectrum is a vibrational spectrum of a molecule. As in the case of infrared spectroscopy, the utility of the Raman spectrum lies in the fact that the vibrational spectrum of a molecule is a sensitive indicator of their chemical properties.

Raman spectra of specimens were obtained using a WiTec Alpha 300R (LOT Oriel, UK) operating a 0.3 W single frequency 785 nm diode laser (Toptica Photonics, Germany) and an Acton SP2300 triple grating monochromator/spectrograph (Princeton Instruments, USA) over the wavenumber range 0 – 3,000 $cm^{-1}$ at a mean resolution of 3 $cm^{-1}$. Mean spectra were composed of a minimum of 500 accumulations, acquiring individual spectra using an integration time of 0.5 s.

### 2.7 Cutting and Hot mounting of glass

All the samples were cut to small pieces using the cutting machine Struers Accutom-5 and a blade exclusively for glass ceramics. The samples were subsequently transferred into the hot mounting machine OPAL 400 (using bakelite) in order to make SEM samples which then were ready for polishing.

### 2.8 Polishing of glass-ceramic samples

For the polishing of the samples, a DAP-7 and Pedemin-S polishing machines were used as well as four different polishing discs: Piano, Largo, Chem and Dac. Three samples were placed in the polishing machine each time and the first polishing disc to be used was the Piano. Water was used as a lubricant for the use of Piano and this disc was used until the sample was plane. Piano was used with about 5-15 N and it lasted for approximately 10 minutes. After that Largo was used with a liquid diamond

suspension with a particle size of 9 microns. The load for Largo was about 5-15 N and it lasted almost 7 minutes Dac was again used with a load of 5-15 N and the lubricant used was a liquid diamond suspension with a particle size of 3 microns. The duration of the polishing with Dac was about 7 minutes. Finally, Chem was once again used with a load of 5-15 N with a liquid diamond suspension with a particle size of less than 1 micron and lasted for about 7 minutes.

### 2.9 X-ray powder diffraction (XRD)

X-ray Powder Diffraction is used in order to measure the crystal size of the formed fluorapatite as well as how the crystal size is affected by zinc substitution. Also, this technique will show the different crystal phases formed with magnesium substitution. An increase in temperature of $10^{o}$C per minute up to $1100^{o}$C using a ramp heated all the frit glass samples. Once that temperature was achieved the samples were left to heat for an hour and then cooled to room temperature using a furnace. X-Ray diffraction was then performed on the samples using a continuous scan between $2\theta = 10°$ and 60°, with a step size of $2\theta = 0.0200°$. A Philips analytical X-Pert XRD was used with Cu Ka, at 40 kV and 40 mA.

The crystal size D was calculated by the Scherrer equation: [30, 31, 64]:

$$D = K\lambda / [w\cos(\theta)] \qquad (\text{Eq } 2.3)$$

where K is a constant that takes values between 0.9 and 1.0 depending on the particle morphology. $\lambda$ is the Cu K$\alpha$ radiation (0.15406nm), w is the full width at half-maximum (FWHM in radian), and $\theta$ is the diffraction angle (in degrees). In this experiment the average value of K = 0.95 was used giving an average volume of the apparent size independent of the morphology.

## 2.10 ESEM- environmental scanning electron microscope and EDX- energy dispersive X-ray analysis

This is a scanning electron microscope (SEM) that allows a gaseous environment in the specimen chamber. The Environmental Scanning Electron Microscope (ESEM) retains all of the performance advantages of a conventional SEM without the high vacuum constraint on the sample environment. The ESEM offers high resolution secondary electron imaging in a gaseous environment, at pressures as high as 6600 Pa, and temperatures as high as 1500°C.

Hence, these detectors produce the highest possible signal-to-noise-ratio at the lowest possible accelerating voltage, because the BSE do not dissipate any energy in an aluminum coating used for the vacuum SEM.

Energy dispersive x-ray analysis is a method used for qualitative and some times quantitative analysis of the elements present in a material. This is achieved when an electron beam gives rise to the characteristic x-ray from a material.

An XL 30 ESEM&EDX FEG electron microscope was used in order to investigate the morphology of the glasses operated at 20 kV. The analysis took place under conditions of high vacuum. The top of the samples was coated with carbon, due to the fact that they lacked conductivity. They were glued onto a small stand and silver paint was used from the edge of the coating till the stand so that the whole of the sample was conductive.

## 2.11 Thermogravimetric analysis (TGA)

Thermogravimetric analysis or thermal gravimetric analysis (TGA) is a type of testing that is performed on samples to determine changes in weight in relation to change in temperature. Such analysis relies on a high degree of precision in three measurements: weight, temperature, and temperature change.

In this study, the instrument used was a NETZSCH Thermal Analysis STA 449C with pairs of matched platinum-rhodium crucibles, and all the runs were performed on 20 mg samples in dry argon at a heating rate of $10^{o}$C/min. The analysis was a direct performance of variation of the weight loss during the heat-treatment.

# CHAPTER 3: RESULTS AND DISCUSSION

## 3.1 Characterisation of glass compositions

### 3.1.1 Density and Oxygen Density of Zn Substituted Glasses

The measured density and oxygen density for zinc containing alumino-silicate glasses are shown in Figures 3.1.1 and 3.1.2. It is indicated, that the density increases proportionally with zinc substitution with the lowest density for LG26 ($4.5SiO_2$-$3Al_2O_3$-$1.5P_2O_5$-$3CaO$-$2CaF_2$) at 2.73 g/cm$^3$ and the highest density for LG26 75% Zn ($4.5SiO_2$-$3Al_2O_3$-$1.5P_2O_5$-$3ZnO$-$0.75ZnF_2$-$1.25CaF_2$) at 3.03 g/cm$^3$. However, the oxygen density, based on the density values mentioned above, does not change significantly, suggesting that there is no significant change observed in the oxygen environment within the glass network with Zn substitution.

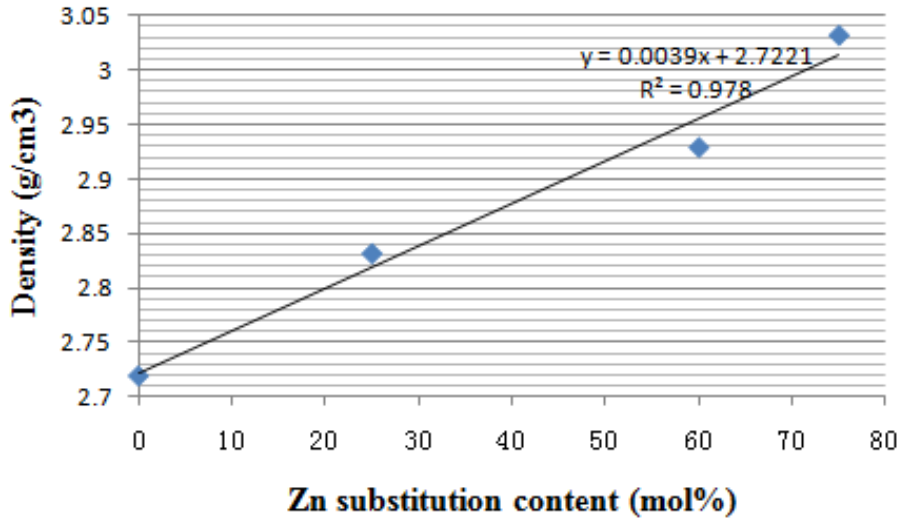


**Figure 3.1.1**: Density of zinc containing glasses.

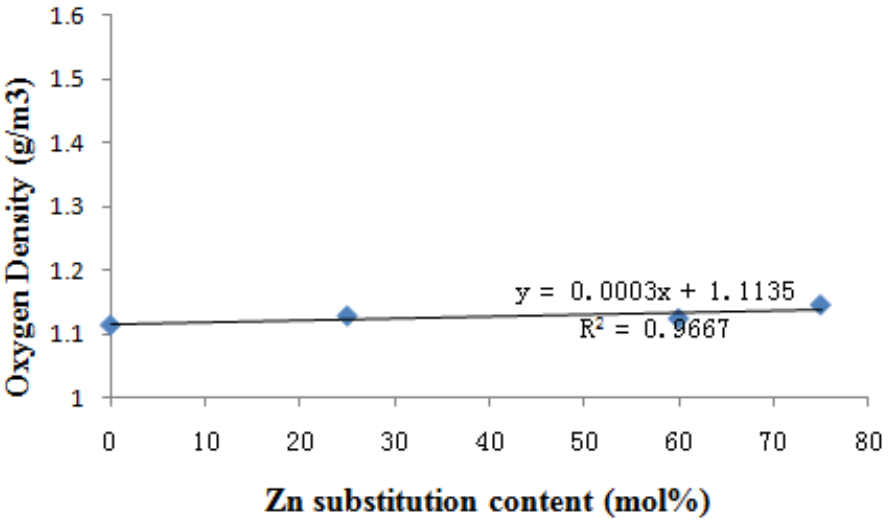


**Figure 3.1.2**: Oxygen density of zinc containing glasses.

The measured density values are increased linearly with increasing the molar content of zinc from 2.73 g/cm3 of LG26 containing glass to 3.03 g/cm3 of LG26 75%Zn containing glass shown in Figure 3.1.1. The substitution of zinc for calcium increases the density of glass as zinc has a larger atomic weight (AW=65.3) than the atomic weight (AW=40) of calcium although the ionic radius of Zn (134pm) is significantly smaller than the ionic radius of calcium (197pm). Since the atomic weight of zinc and calcium are significantly different, the linear increase of density indicates that the atomic weight change has a more important effect on the density values than the ionic radius.

Concerning the oxygen density, the measured values increased as the zinc substitution increased, as shown in the Figure 3.1.2. The minimum value is 1.113 g/cm3 for the case of LG26 and the maximum value appears in 1.168 g/cm3 in the case of LG26 75%Zn. In the glass network, the oxygen density reflects the degree of packing of the atoms. There is a slight linear increase in the oxygen density from LG26 to LG26 75%Zn containing glasses indicating a closer packed glass network. It is clear that zinc substitution leads to an increase in glass density and an increase in oxygen density. Consequently, it was observed that zinc substitution leads to an increase in glass density and an increase in oxygen density.

### 3.1.2 FTIR analysis of Zn substituted glasses

Figure 3.1.3 shows the FTIR absorbance spectra of all zinc containing glasses. The first strong bands in the region of 800-1400 cm-1 appear in all samples and are assigned to the Si-O(s) and P-O(s) stretching vibrations [81, 82], however with increasing the zinc molar content from LG26 to 60% , these bands are shifted to slightly higher wavenumbers, ie., from 1095 $cm^{-1}$ to 1105 $cm^{-1}$. In addition, there is an effect in the intensity of the band situated at around 983 $cm^{-1}$ and the intensity decreased with increasing the zinc molar content in the glass. Furthermore, there is a medium strong band in the region of 620-800 $cm^{-1}$ which is associated with $AlO_4$ tetrahedra. The band between 530-620 $cm^{-1}$ is attributed to the P-O bending vibrations and Si-O-Al linkages, while the band centred at around 452 $cm^{-1}$ is related to the motion of bridging oxygens in the plane perpendicular to the Si-O-Si(Al) bond and is attributed to the vibrations of Si-O-Si and Si-O-Al bonds [83- 85].

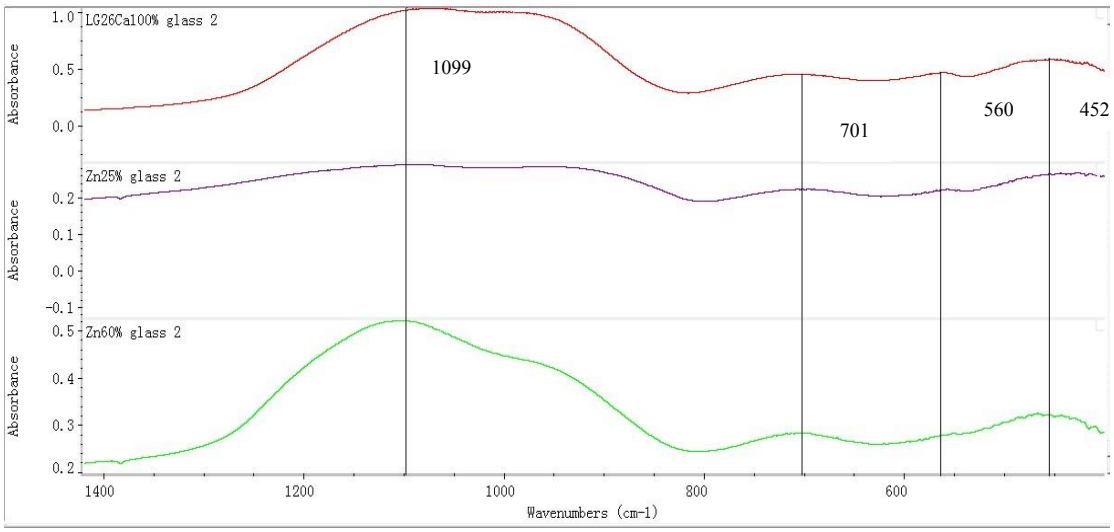


**Figure 3.1.3**: FTIR spectra of zinc substituted glasses.

**Table 3.1.1:** Assignment of FTIR peaks in zinc substituted glasses.

| *Wavenumber ($cm^{-1}$)* | *LG26 100%Ca* | *LG26 25%Zn* | *LG26 60%Zn* | *Description* |
|---|---|---|---|---|
| | 400-530 | 400-530 | 400-530 | Si-O-Si (Al) bending vibrations [83] |
| | 530-620 | 530-620 | 530-620 | P-O bending and Si-O-Al linkages [81] |
| | 620-800 | 620-800 | 620-800 | Al-O stretching vibrations with aluminium in four-fold coordination [84] |
| | 800-1400 | 800-1400 | 800-1400 | Si-O (s) stretching vibrations with a different number of bridging oxygen atoms [85] |

Fourier transform infra-red spectroscopy can provide information concerning the chemical structure of our glasses. An example of an FTIR study is the one conducted by Stoch et al. [81] on glasses containing $SiO_2$, $Al_2O_3$, $B_2O_3$ and $P_2O_5$. The presence of aluminium in the silicate network usually causes a shift of the bands to smaller wavenumbers. There appears to be a band at about 980 $cm^{-1}$ which is characteristic for ortho-silicates. The presence of $P_2O_5$ causes the appearance of a band at 1330 $cm^{-1}$ due to the P=O bonds and the stretching and vibration mode of Si-O-P and P-O-P bonds. The main band at 1100-1220 $cm^{-1}$ is caused by the Si-O-Si. At 800 $cm^{-1}$, the band is caused by Si-O-P stretching vibrations. Depending on the amount and type of network modifiers ($Na^+$, $Ca^{2+}$, or $Zn^{2+}$), the position of the Si-O-Si band which is normally at 1100 $cm^{-1}$ varies. The vibrations of Al-O-P bridges are usually seen at the range of 1100-1200 $cm^{-1}$ and in some glasses they seem to overlap with the Si-O-Si band.

In another study conducted on ionomer glasses by Nourmohammadi et al. [86], a band at 1050 $cm^{-1}$ was found to correspond to the Si-O-Si stretching vibrations and another band at 950 $cm^{-1}$ was found to correspond to the Si-OH deformation vibrations.

The lack of sharp peaks in the FTIR spectra indicates a disorder in the silicate network reflecting the wide distribution of $Q^n$ units occurring in the glasses. J. Serra et al. [59] reported that the bending Si-O(b) vibrations were identified around 800 $cm^{-1}$ and the asymmetric stretching mode Si-O(s) was located in the range of 100-1300 $cm^{-1}$. It was also reported that the symmetric and asymmetric stretching modes of Si-O-Si bonds in the $Q^n$ units appeared in the 800-1300 $cm^{-1}$ region with the absorption bands of the $Q^n$ units with n= 4, 3, 2, 1 and 0 centred around 1200, 1100, 950, 900 and 850 $cm^{-1}$, respectively [82]. As reported from the literature [83] in a simple silica glass all the silicon atoms are bonded to four oxygen atoms and all oxygen atoms are bridging oxygen atoms (BO), each oxygen atom bridges two silicon atoms. Convention refers as well that in FTIR spectra, the main absorption band is in the range of 800-1400 $cm^{-1}$, which indicates a distribution of Si-O-Si stretching ($Q^4$), Si-O-Si stretching ($Q^3$) and Si-O-[NBO] per $SiO_4$ tetrahedron ($Q^3$) [83, 84]. Zn acting as a network modifier can induce a visible shift of certain bands indicating a change of formation of non-bridging oxygens in the glass network. It was observed that, when Zn concentration increased, the position of both Si-O-Si stretching ($Q^3$) (1099$cm^{-1}$) and Si-O-[NBO] bands (980$cm^{-1}$) shifted towards higher values (1105$cm^{-1}$ and 985$cm^{-1}$, respectively), and the intensity of the band associated with Si-O-[NBO] generally decreased. The declination of the intensity of Si-O-[NBO] suggests that there was more Si-O-Si as well as bridging-oxygens formed in the glass network. The formation of more Si-O-Si bonds and the decrease of Si-O-NBOs play an important role in the biological response at the interface of bioactive materials when exposed to body fluids, therefore the study of the bonding configuration is a key step for the development of new glasses and their biomedical application [85].

### 3.1.3 Raman analysis of zinc substituted glasses

The zinc substituted glasses were investigated by polarized Raman scattering. Vibrational modes were assigned to different types of atomic motion in the glass network. Table 3.1.2 presents the spectral band positions that have been discussed in the literature for alumino silicate glasses. The bands below 400 $cm^{-1}$ have been attributed to the low-lying optic and high-lying acoustic modes in the glass network ($\leq$100$cm^{-1}$) [87, 88] and to the cation motion relative to the silicate network (100-400$cm^{-1}$) resulting from the symmetric motion of bridging oxygens relative to silicon atoms in the three-dimensional network structure ($\nu_s$(Si-O-Si)) [89]. An intense peak around 540 $cm^{-1}$ has been assigned to symmetric aluminium tetrahedra network with four oxygens in a bridging configuration, and the weak Raman peak around 767 $cm^{-1}$ has been assigned to $[AlO_4]^-$ tetrahedra with three bridging and one non-bridging oxygens [90, 91]. In addition, a peak at 710 $cm^{-1}$ has been attributed to the presence of octahedral aluminium in the glass network [92]. Furthermore, the bands in the region of 900-1200 $cm^{-1}$ are due to highly localized Si non-bridging oxygen stretching modes and the relative intensities of these bands may be used to determine cation distributions around $SiO_4$ tetrahedra [93].

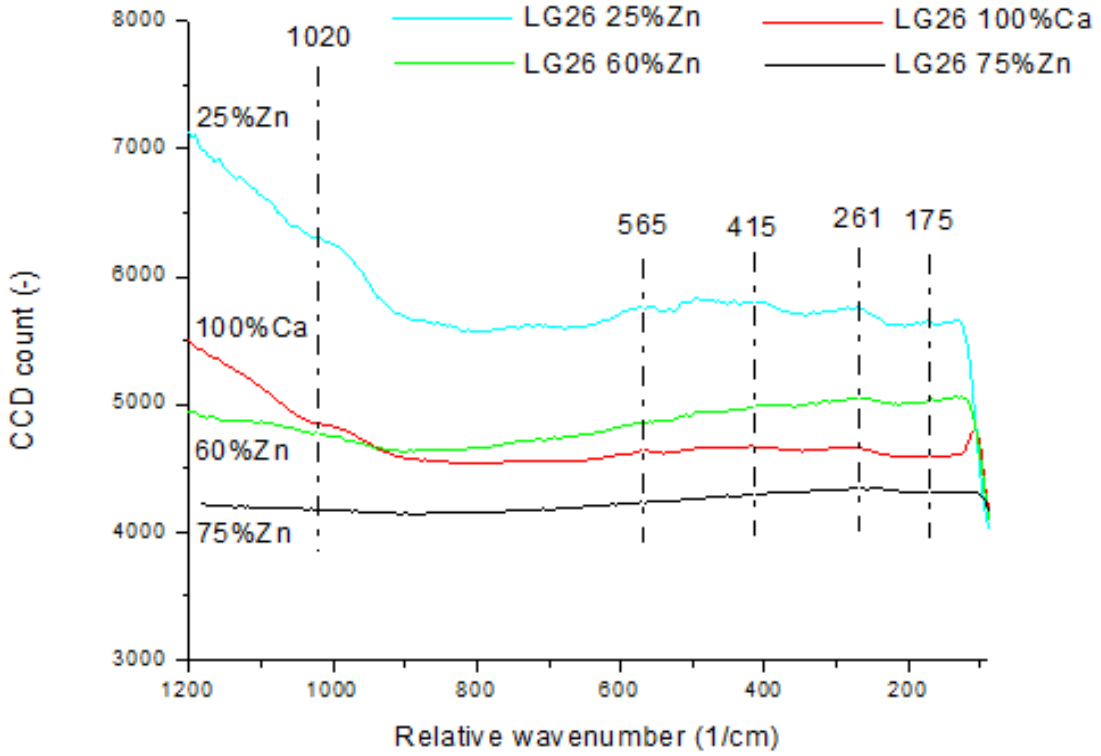


**Figure 3.1.4**: Raman spectra of zinc substituted glasses.

**Table 3.1.2:** Assignment of Raman peaks in alumino silicate glass networks from the literature.

| *Wavenumber ($cm^{-1}$)* | *Description* |
|---|---|
| 100-400 | Silicon atoms in the three-dimensional network structure ($\nu_s$(Si-O-Si)) [89] |
| 500-800 | Symmetric $AlO_4^-$ tetrahedral network [90,91] |
| 900-1200 | Si-NBO stretching modes [93] |

The Raman spectra of glassy silicate materials are characterized by a number of broad features reflecting the multiple coordination of Si–O bonds. Colomban [94] described this complex picture invoking several types of chain, sheet and three-dimensional structures labelled $Q^0$–$Q^4$, which can be assigned as follows: $Q^0$, representing monomer $SiO_4$ units, with bands in the region 850–800 $cm^{-1}$; $Q^1$, representing $Si_2O_7$ groups, with a band near 950$cm^{-1}$; $Q^2$, silicate chains with bands in the region of 1100–1050 $cm^{-1}$; $Q^3$, silicate sheets with a band near 1100$cm^{-1}$; and $Q^4$,

representing $SiO_2$ and tectosilicates with a band in the range of 1250–1150 $cm^{-1}$ [95]. It is worth noticing, that the current spectra were very broad and often the peaks seemed to be overlapping.

### 3.1.4 DSC and TGA thermal analysis

Tables 3.1.3 and 3.1.4 present the glass transition temperature, the crystallization temperatures and the crystal dissolution temperatures of all fine (<45μm) and coarse powder glasses (>45 and <100μm), respectively. The crystal dissolution temperature appeared in the DSC graphs shown in Figures 3.1.5-3.1.8 as an endothermic transition (discussed below) that looked very similar to a melting point but could not be considered as the melting point of glasses as it was far too low to the actual melting point of the glass.

**Table 3.1.3**: DSC analysis data for all Zn containing fine powder glasses measured at a heating rate of 10°C/min.

| **Glass (fine powder)** | **Zn content (molar %)** | **$T_g$(°C )** | **$T_{p1}$(°C )** | **$T_{p2}$(°C )** | **Crystal dissolution temperature (°C)** |
|---|---|---|---|---|---|
| **LG26 Ca100%** | 0 | 655 | 751 | 934 | ---- |
| **LG26Zn25%** | 25 | 625 | 842 | 947 | 1161 |
| **LG26Zn60%** | 60 | 616 | 943 | ---- | 1160, 1185 |
| **LG26Zn75%** | 75 | 595 | 876 | ---- | 1244 |

**Table 3.1.4**: DSC analysis data for all Zn containing coarse powder glasses measured at a heating rate of 10°C/min.

| Glass (coarse powder) | Zn content (molar %) | $T_g$(°C ) | $T_{p1}$(°C ) | $T_{p2}$(°C ) | Crystal dissolution temperature (°C) |
|---|---|---|---|---|---|
| **LG26Ca100%** | 0 | 667 | 793 | 1008 | ---- [98] |
| **LG26Zn25%** | 25 | 627 | 933 | 1032 | 1173 |
| **LG26Zn60%** | 60 | 613 | ---- | ---- | 1188 |
| **LG26Zn75%** | 75 | 616 | ---- | ---- | 1255 |

From Table 3.1.3 it is clear that the glass transition temperature decreased with zinc substitution. The first crystallization temperature increased with substitution with the exception of the 75% Zn substitution where a small decrease was observed compared to the 60% Zn substitution. It is interesting to note, that the second crystallization temperature did not show significant change. The crystal dissolution temperature exhibited a slight increase with zinc substitution. From Table 3.1.4 on the other hand we can see that the glass transition temperature of the coarse particle glasses does not change significantly with substitution whereas no crystallization temperatures were recorded for 60 and 75% Zn substituted glasses. Since crystal dissolution temperatures were recorded one could think that crystallization occurred very slowly. For this reason isothermal measurements were conducted at 900, 950 and 1000°C. The DSC graphs are shown in Figures 3.1.13-3.1.19. And it is indicated from Table 3.1.4 that the transition temperature not changes much and the crystallization temperature is 1000°C and 950°C for LG26 60% and 75% coarse glasses. All graphs show one glass transition temperature, one or two crystallization peak temperatures and another endothermic transition during which a small weight loss was observed in the TGA analysis shown in Figures 3.1.9 to 3.1.12. One speculation could be that this transition is not associated with melting but with crystal dissolution (CD) during

which some loss of weight is observed due to a surface loss of $SiF_4$ from the glass particles. $SiF_4$ loss has not been proved experimentally however it is expected that some very small loss occurs during glass making as well as during heat treatments.

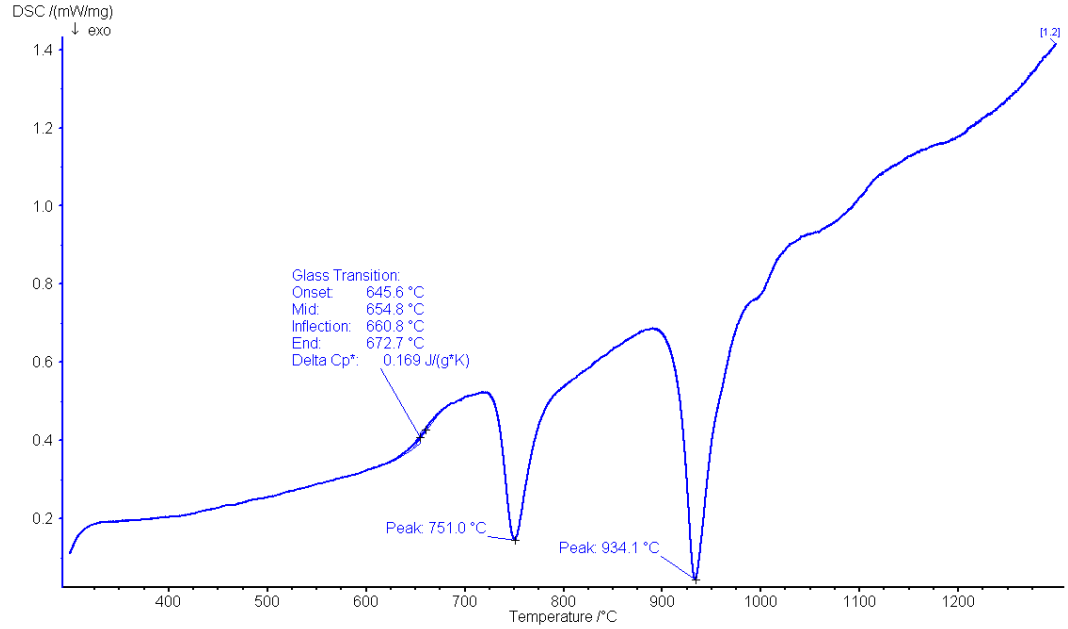


**Figure 3.1.5**: DSC trace of calcium containing glass LG26 100%Ca glass with particle size <45µm measured at a heating rate of 10°C/min.

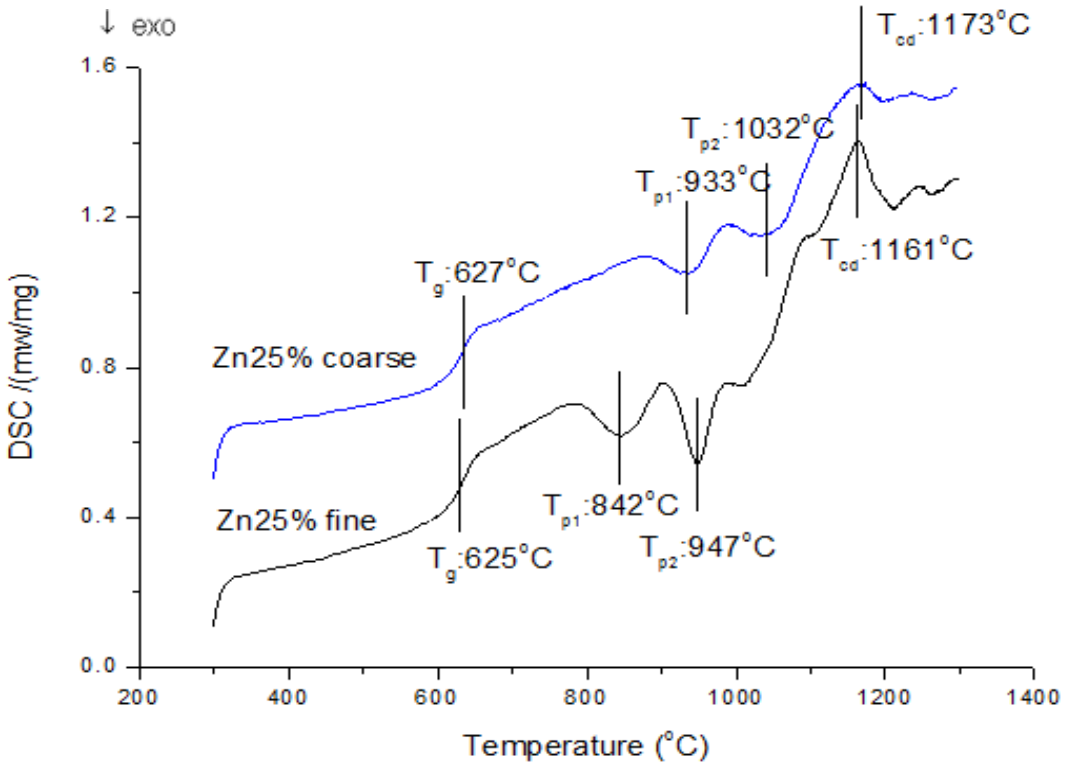

**Figure 3.1.6**: DSC traces of zinc substituted glass LG26 25%Zn glass having different particle size (coarse 45-100µm and fine <45µm) measured at a heating rate of 10°C/min.

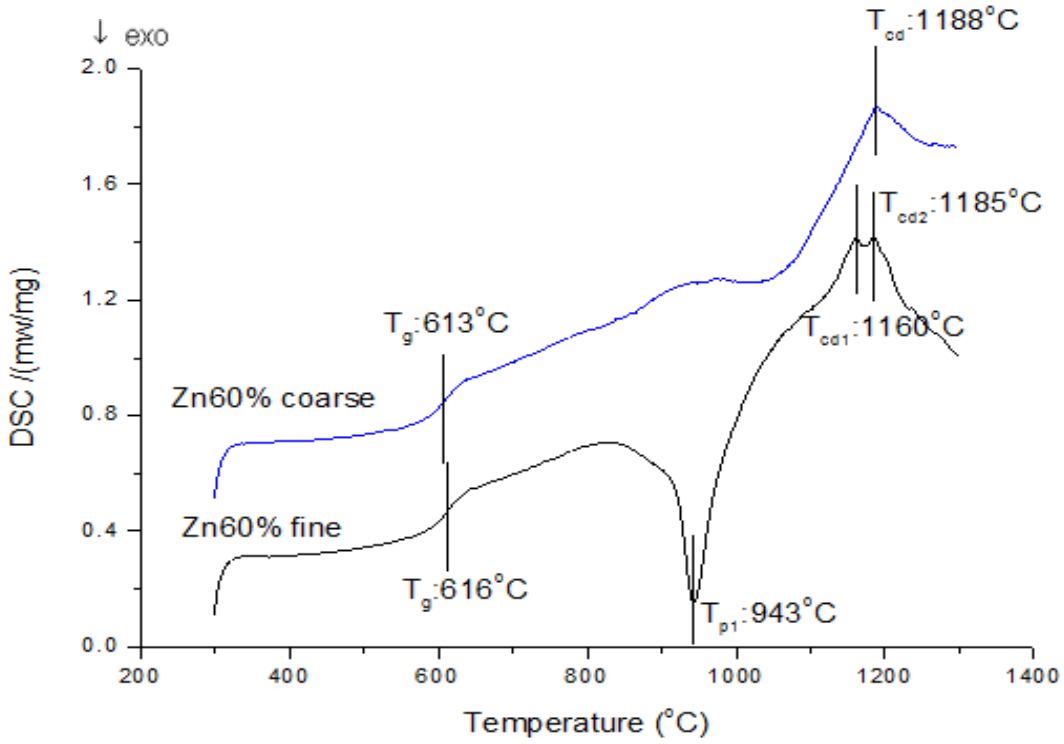


**Figure3.1.7**: DSC traces of zinc substituted glass LG26 60%Zn glass having different particle size (coarse 45-100µm and fine <45µm) measured at a heating rate of 10°C/min.

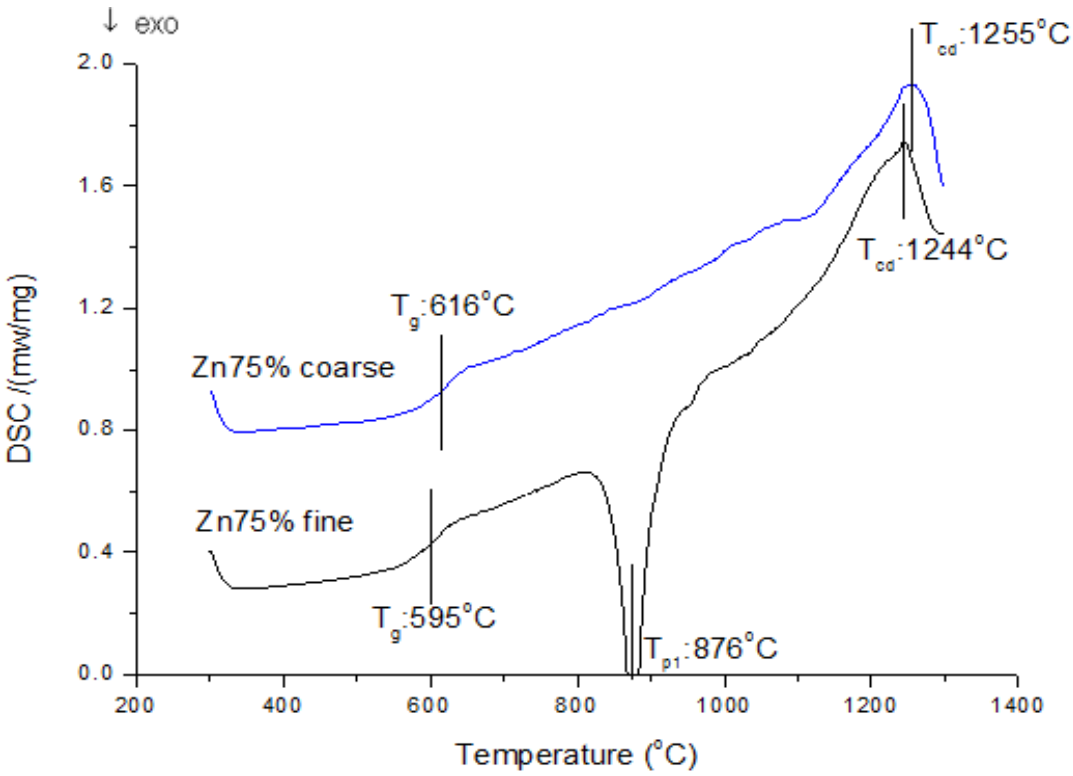


**Figure 3.1.8**: DSC traces of zinc substituted glass LG26 75%Zn glass having different particle size (coarse 45-100μm and fine <45μm) measured at a heating rate of 10°C/min.

In Table 3.1.5 is clear, that weight loss in glasses occurred in two stages: The temperature at which the first weight loss was recorded was 750 to 662°C whereas the temperature at which the second weight loss (total 0.2%) was recorded was around 1000°C. Above this temperature, the weight loss that was recorded for all glasses was 1.25% with the exception of LG26 75%Zn of which the weight loss increased to 2.3%. Generally, only a small weight loss was recorded for all glasses with the 75% Zn substituted glass to have the highest. It is worth noticing, that all the thermogravimetric analysis was conducted on fine powder glass samples and it was expected that if there was a weight loss this should be due to the larger surface area. It is suggested, that there is a small fluorine loss from the surface of the glasses due to possibly $SiF_4$ formation during heating. This however cannot been proved based on the data that are available in this work.

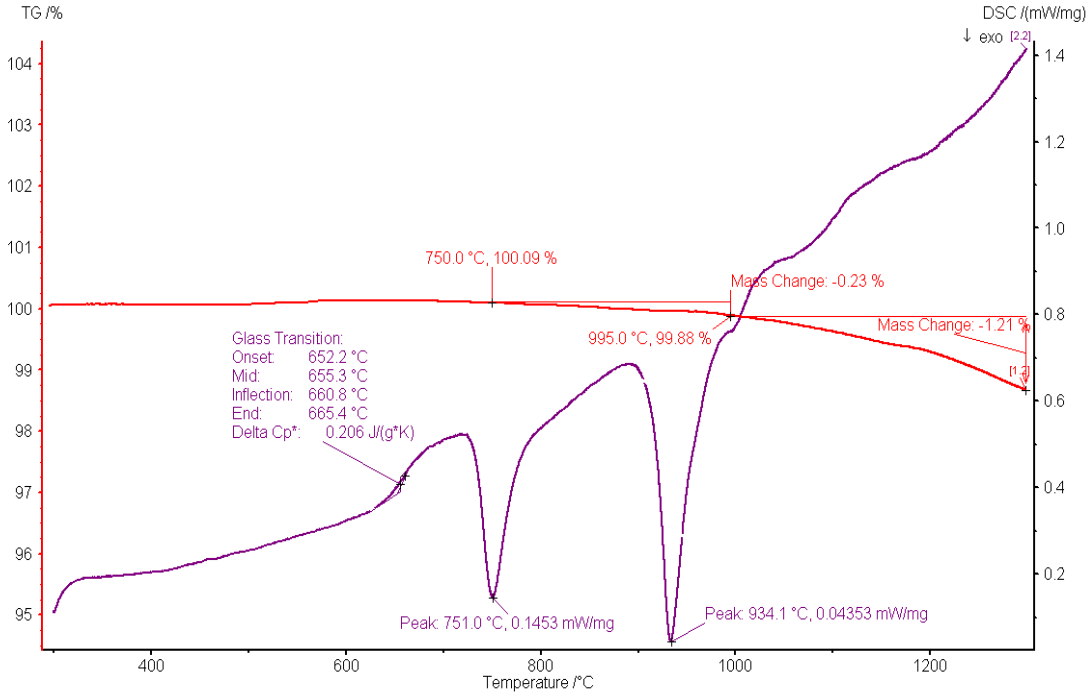


**Figure 3.1.9**: TGA analysis on Ca100% LG26 glass.

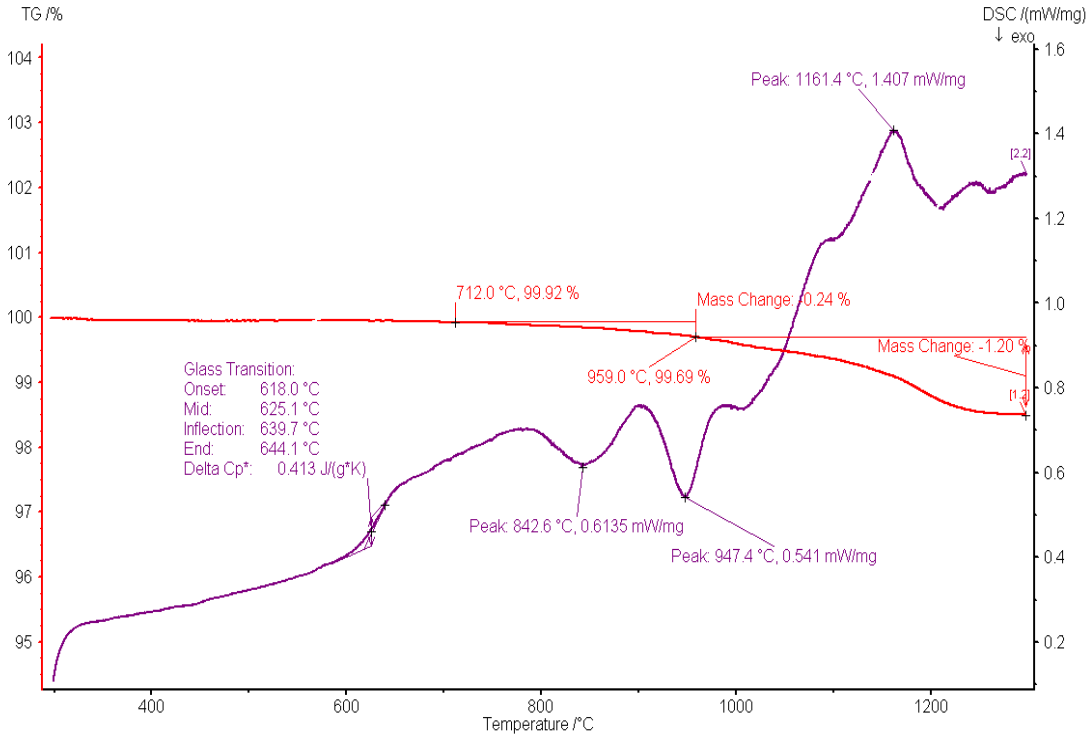


**Figure 3.1.10**: TGA analysis on Zn25% LG26 glass.

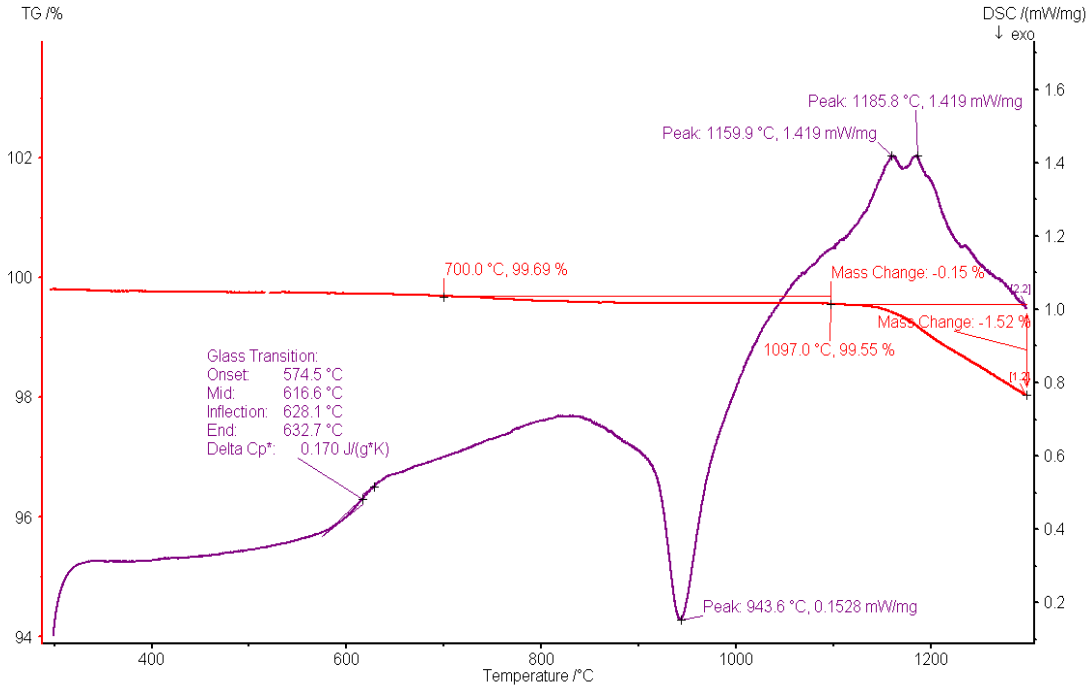


**Figure 3.1.11**: TGA analysis on Zn60% LG26 glass.

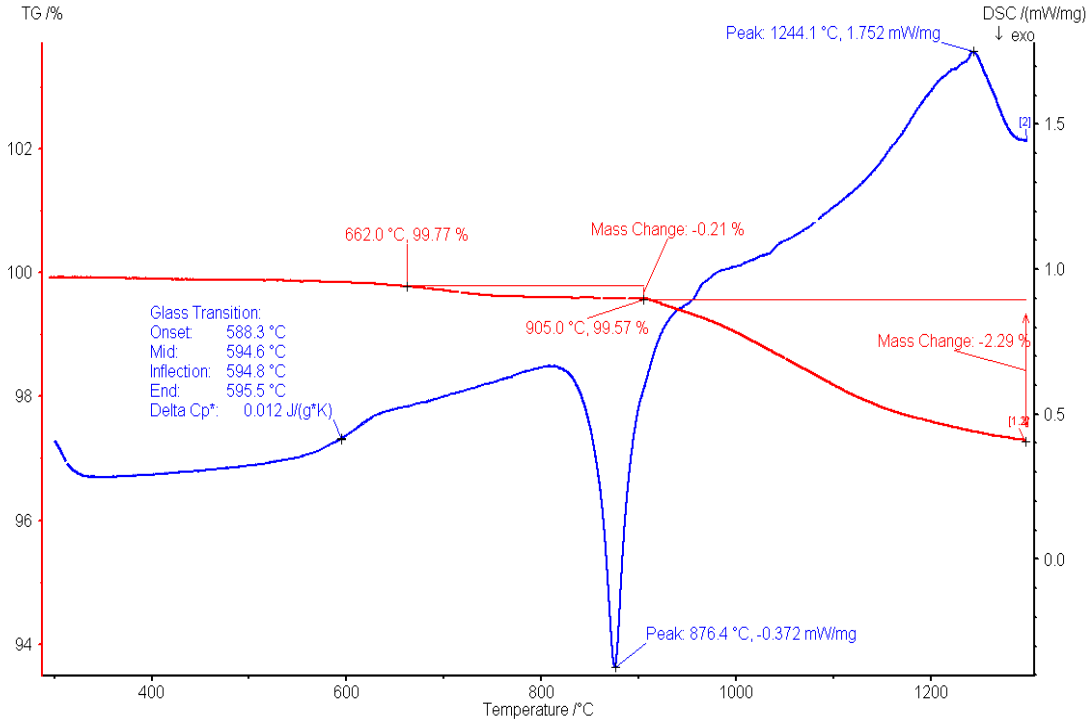


**Figure 3.1.12**: TGA analysis on Zn75% LG26 glass.

**Table 3.1.5**: Thermogravimetric analysis of zinc substituted glasses.

| Glass | Weight loss start temperature ($^{o}$C) | Weight loss (%) | Weight loss second temperature ($^{o}$C) | Weight loss (%) |
|---|---|---|---|---|
| **LG26 100%Ca** | 750 | 0.20 | 970 | 1.21 |
| **LG26 25%Zn** | 712 | 0.24 | 960 | 1.20 |
| **LG26 60%Zn** | 700 | 0.15 | 1097 | 1.52 |
| **LG26 75%Zn** | 662 | 0.21 | 905 | 2.29 |

Figures 3.1.13 to 3.1.16 show the isothermal studies at 950 and 1000$^{o}$C, that were conducted for LG26 60%Zn and LG26 75% Zn glasses. It is clear, that both glasses exhibited a sharp exothermic peak around 1000$^{o}$C and 950$^{o}$C, respectively. It is interesting to note that the glasses crystallized very early in the heat treatment.

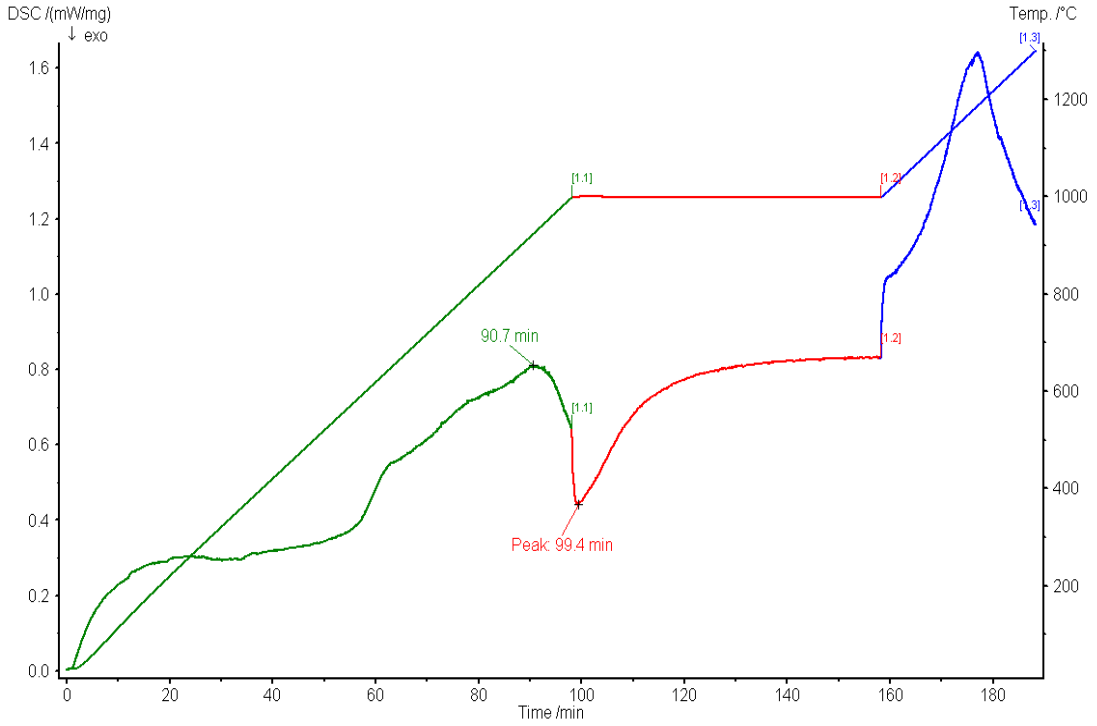


**Figure: 3.1.13**: Isothermal DSC curve of LG26 60%Zn (coarse glass). 1 hour hold at 1000$^{o}$C.

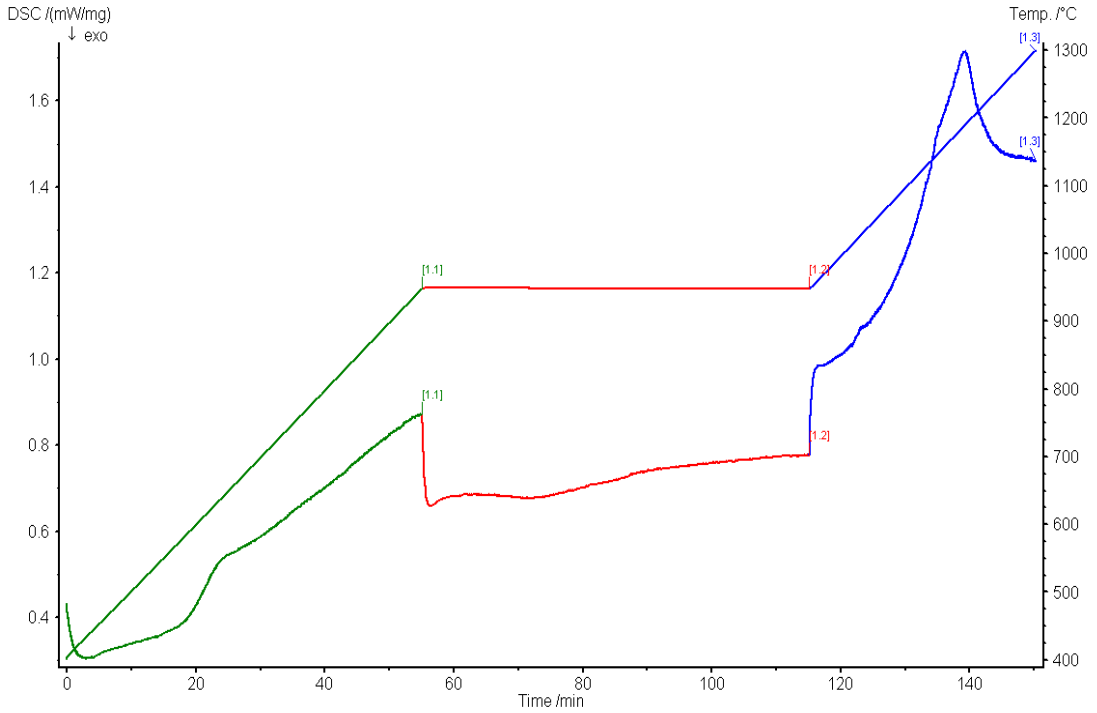


**Figure 3.1.14**: Isothermal DSC curve of LG26 60%Zn (coarse glass). 1 hour hold at 950°C.

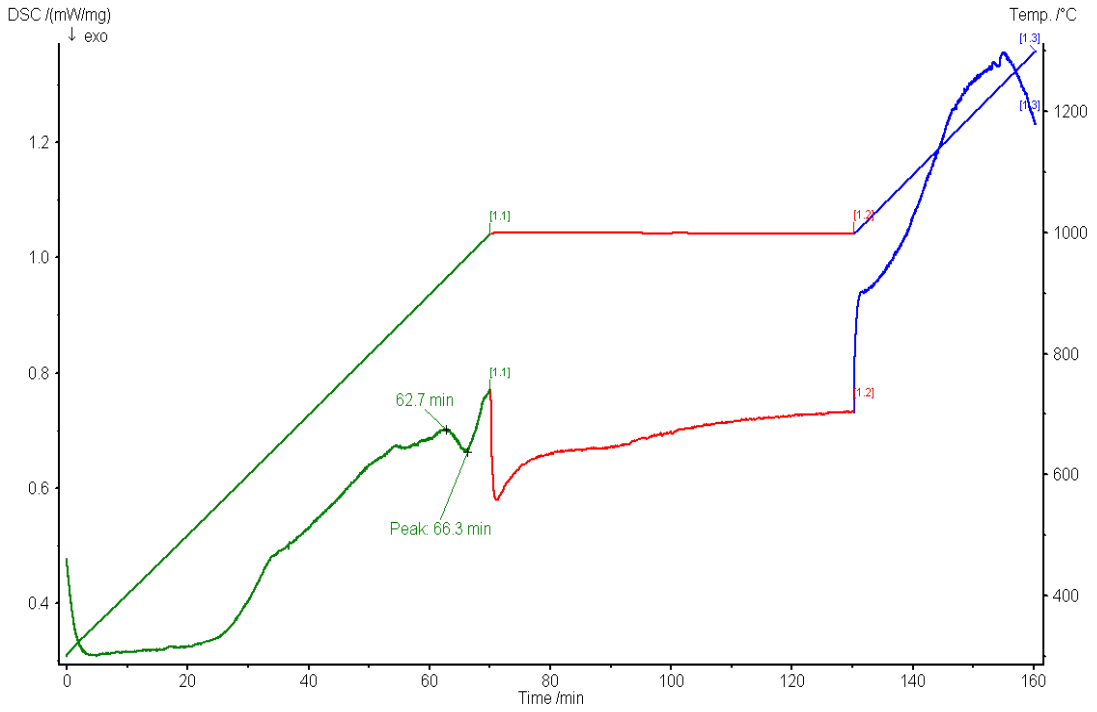


**Figure 3.1.17**: Isothermal DSC curve of LG26 75%Zn (coarse glass). 1 hour hold at 1000°C.

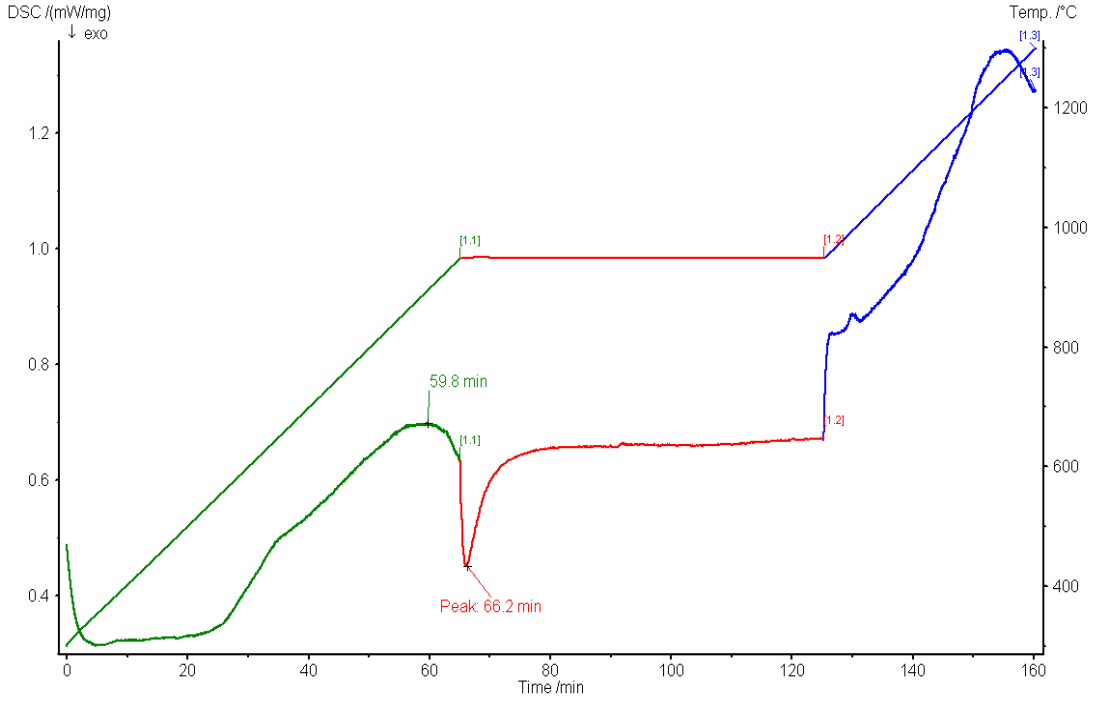


**Figure 3.1.18**: Isothermal DSC curve of LG26 75%Zn (coarse glass). 1 hour hold at 950°C.

**Table 3.1.6**: Isothermal analysis of LG26 60%Zn coarse glass and LG26 75%Zn coarse glass.

| **Glass (coarse powder)** | **Zn content (molar %)** | **$T_g$(°C )** | **$T_{p1}$(°C )** | **$T_{p2}$(°C )** | **Crystal dissolution temperature (°C)** |
|---|---|---|---|---|---|
| **LG26Zn60%** | 60 | 613 | 1000 | ---- | 1188 |
| **LG26Zn75%** | 75 | 616 | 950 | ---- | 1255 |

Figures 3.1.5 to 3.1.8 present the DSC curves of LG26 zinc substituted glasses. Table 3.1.3, 3.1.4 and 3.1.6 present the values of $T_g$, $T_p$ and $T_{cd}$ for all glasses. It is clear that for the fine powder samples, the glass transition temperature ($T_g$) of LG26 Ca100% was the highest at 655°C whereas the $T_g$ of the rest of the glasses (LG26 25%Zn, LG26 60% Zn and LG26 75%Zn) decreased with increasing the zinc content. The

lowest glass transition temperature was 595$^{o}$C for LG26 Zn75% fine glass, suggesting that with increasing zinc content in the glass more zinc ions enter the glass network that affect the glass microstructure and chemical bonding. The question is whether zinc takes part in the glass network formation. We think that most likely not, in the contrary zinc may result to phase separation competing for aluminium with silicon which eventually leads to a decrease in the number of Si-O-Al formation as we can also see from the Raman spectra where the intensities of the peaks in the area around 450 cm$^{-1}$ associated with Si-O-Al linkages decreased with increasing zinc content.

It is interesting to observe, that there are two crystallization temperatures in both 100%Ca and 25%Zn glasses. As reported previously for the 100%Ca glass [16], the first crystallization temperature (around 620$^{o}$C) is due to the fluorapatite formation whereas the second crystallization temperature is due to mullite formation. Similarly, the first crystallization temperature in the 25% zinc substituted glass corresponds to the fluorapatite phase, whereas the second crystallization temperature corresponds to both gahnite and mullite formation. As zinc content increases only one crystallization temperature can be recorded and as mentioned above, the 60% and 75%Zn glasses crystallize to one main phase gahnite. Fluorapatite cannot form and it seems that the glass separates into a zinc aluminium rich phase, a zinc-calcium-phosphorus rich phase and an amorphous silicon rich phase. Crystallization in 60 and 75% glasses seems to be very slow and is mainly surface driven. The 100% zinc substituted glass was not possible to form as it crystallizes rapidly suggesting that most likely zinc disrupts the glass network leading to complete phase separation. The endothermic transition at around 1200$^{o}$C was assumed to be a crystal dissolution temperature and seems to increase with zinc substitution. It is difficult, however to conclude whether the latter is an important information about the glass network based on the data presented here. Unfortunately, the Raman spectra of glasses were not very helpful as the peaks were very broad and the interpretation of the data was based rather on a few assumptions.

**Effect of Particle size on the crystallization of Zn containing glasses studied by DSC**

Zinc containing glasses of different particle size (<45μm and 45-100μm) were studied by DSC analysis from room temperature to 1300$^{o}$C at a heating rate of 10$^{o}$C/min. Bulk crystallization is generally manifested by the independence of the crystallization peak temperatures from the particle size, while the opposite suggests dependence from the surface area and therefore surface crystallization. Previous work suggested that the calcium base glass exhibits mainly bulk crystallization and the crystallization temperatures were not dependent on the particle size of the glass sample. However, the 25% Zn (Figure 3.1.6) substituted glass shows dependency of both crystallization temperatures on the glass particle size, suggesting surface crystallization. Similarly the 60 and 75% Zn (Figures 3.1.7 and 3.1.8) substituted glasses show the same behavior. It is clear, that the zinc substituted glass is different than the calcium base glass and therefore it is expected that the crystallization mechanism and phases formed should be also different.

## 3.2 Effect of Cation Substitution on Glass-Ceramics

### 3.2.1 XRD study of zinc substituted glasses and glass-ceramics

**Table 3.2.1**: Main Crystal phases in zinc substituted glass-ceramics.

| Glass | Crystal phases | | | | |
|---|---|---|---|---|---|
| LG26 100%Ca | $Ca_5(PO_4)_3F$ | $Al_6Si_2O_{13}$ | $AlPO_4$ | X | X |
| LG26 25%Zn | $Ca_5(PO_4)_3F$ | $Al_6Si_2O_{13}$ | $AlPO_4$ | $ZnAl_2O_4$ | X |
| LG26 60%Zn | $Ca_5(PO_4)_3F$ | $SiO_2$ (cristobalite) | $AlPO_4$ | $ZnAl_2O_4$ | $CaZn_2(PO_4)_2$ |
| LG26 75%Zn | X | $SiO_2$ (cristobalite) | $AlPO_4$ | $ZnAl_2O_4$ | $CaZn_2(PO_4)_2$ |

Table 3.2.1 presents the crystal phases formed after the crystallization of glasses. Figure 3.2.1 shows the X-ray diffractogramm of LG26 Ca100% glass. The glass is crystallized mainly to Ca fluorapatite ($Ca_5(PO_4)_3F$) (Ref.Code 00-015-0876) and mullite ($Al_6Si_2O_{13}$) (Ref.Code 00-015-0776). A minor phase is aluminium phosphate ($AlPO_4$) (Ref.Code 00-011-0500). Figure 3.2.2 represents the diffractogramm of the 25% Zn substituted crystallized glass. Gahnite ($ZnAl_2O_4$) (Ref.Code 00-005-0669) and fluorapatite are the major phases whereas $AlPO_4$ is again a minor phase. The diffractogramm of the 60% Zn substituted crystallized glass shown in Figure 3.2.3 suggested that gahnite ($ZnAl_2O_4$) is the major phase whereas calcium zinc phosphate ($CaZn_2(PO_4)_2$) (Ref.Code 00-020-0248), some fluorapatite and cristobalite ($SiO_2$) (Ref.Code 00-011-0695) are also present whereas $AlPO_4$ is again a minor phase.

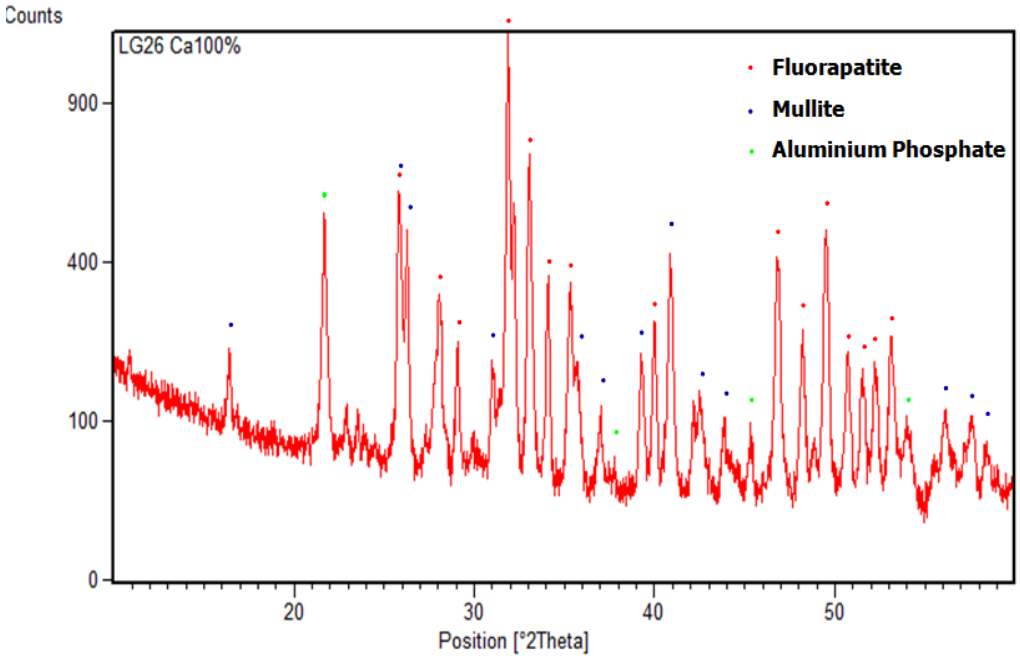


**Figure 3.2.1**: X-ray powder diffraction pattern of LG26 Ca100% glass-ceramic.

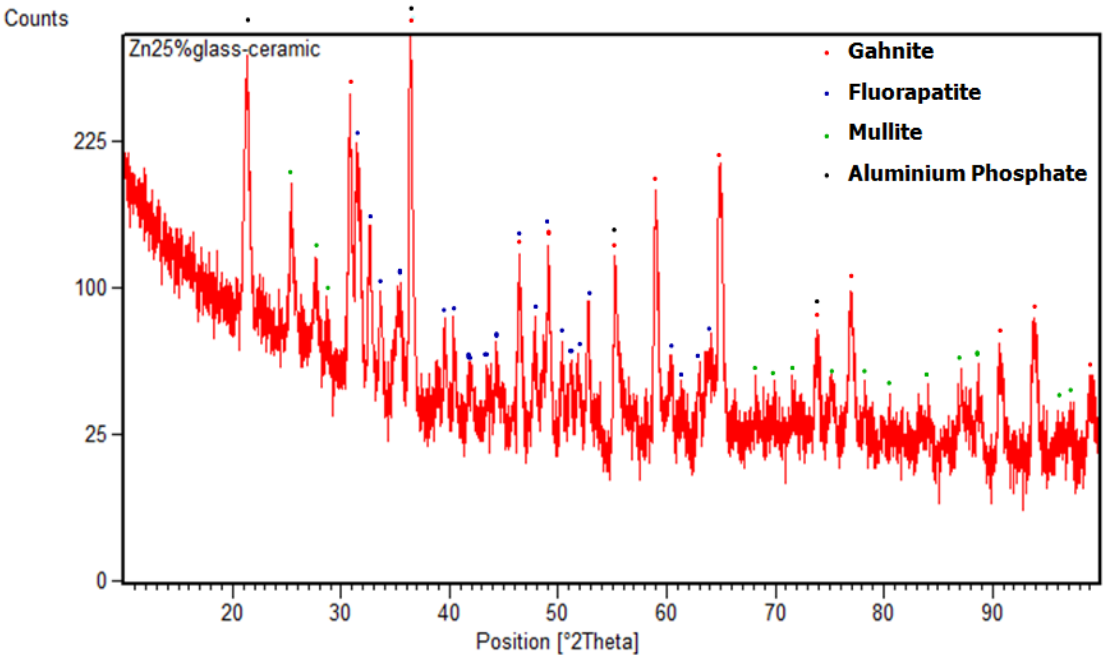


**Figure 3.2.2**: X-ray powder diffraction pattern of LG26 Zn25% glass-ceramic.

Figure 3.3.4 shows the X-ray diffractogramm of LG26 75%Zn crystallized glass and it is suggested that the glass was crystallized to Gahnite, calcium zinc phosphate and a small amount of crystobalite whereas $AlPO_4$ is again a minor phase. X-ray diffraction was conducted for all glasses and it was interesting to see that the 75% Zn substituted glass (Figures 3.2.5 and 3.2.6) showed a few diffraction peaks that corresponded to gahnite whereas all the other glasses were amorphous.

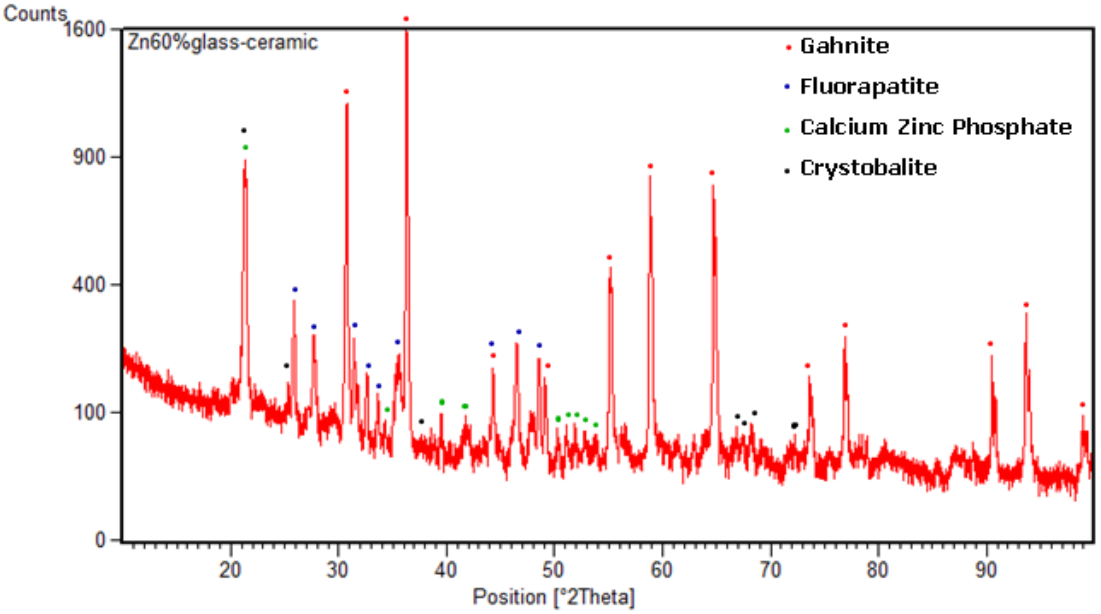


**Figure 3.2.3**: X-ray powder diffraction pattern of LG26 Zn60% glass-ceramic.

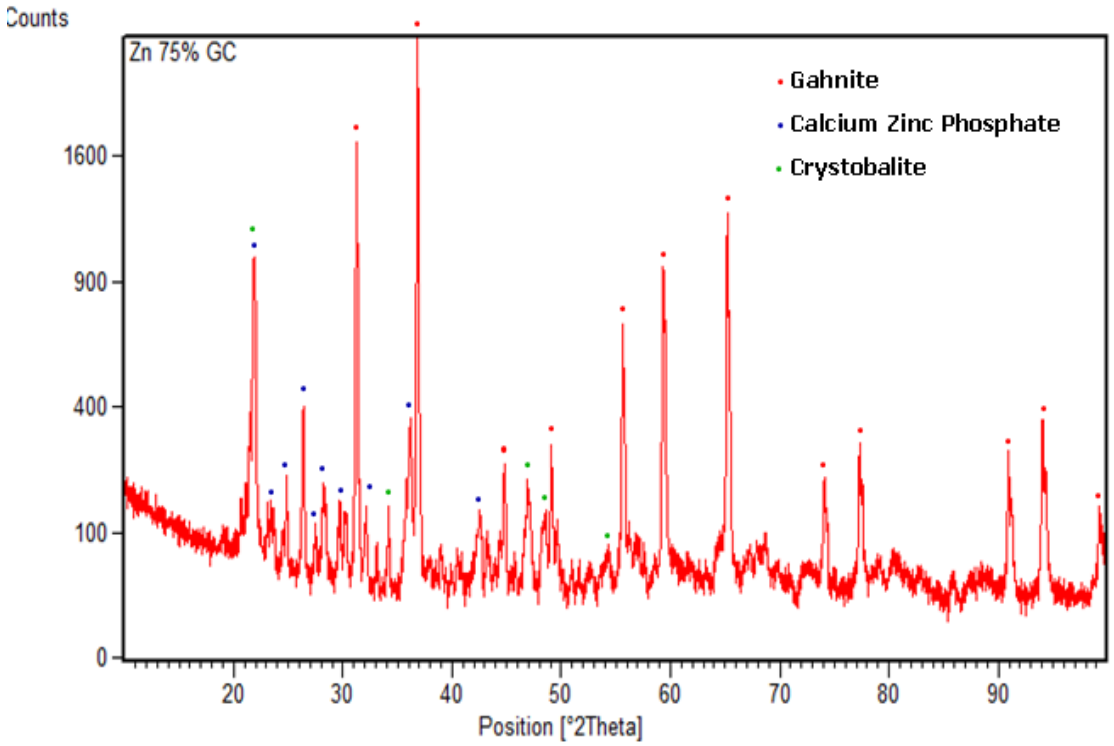


**Figure 3.2.4**: X-ray powder diffraction pattern of LG26 Zn75% glass-ceramic.

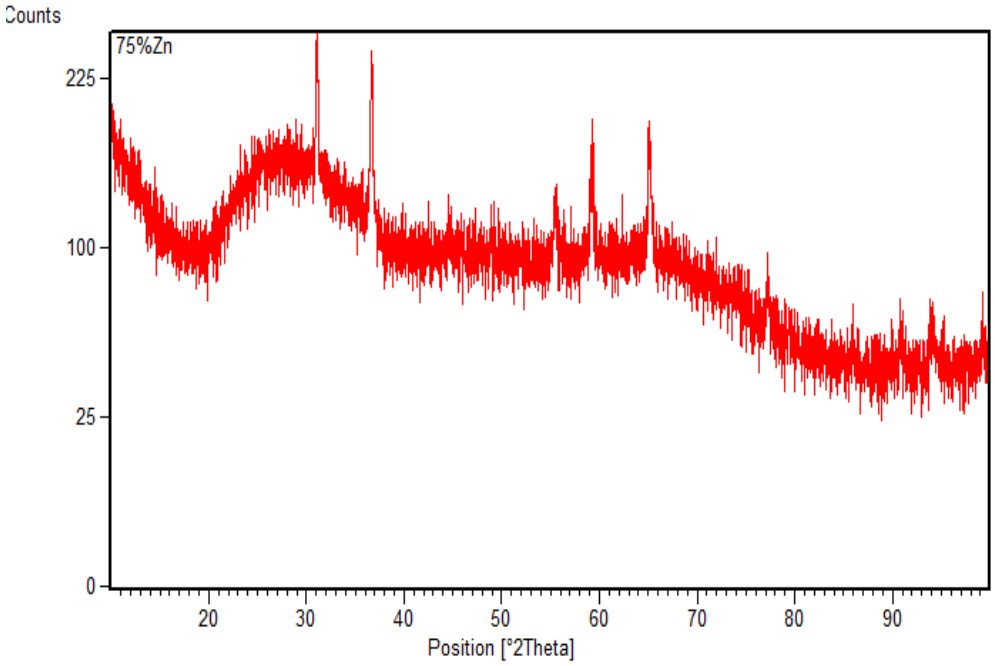


**Figure 3.2.5**: X-ray powder diffraction pattern of LG26 Zn75% glass.

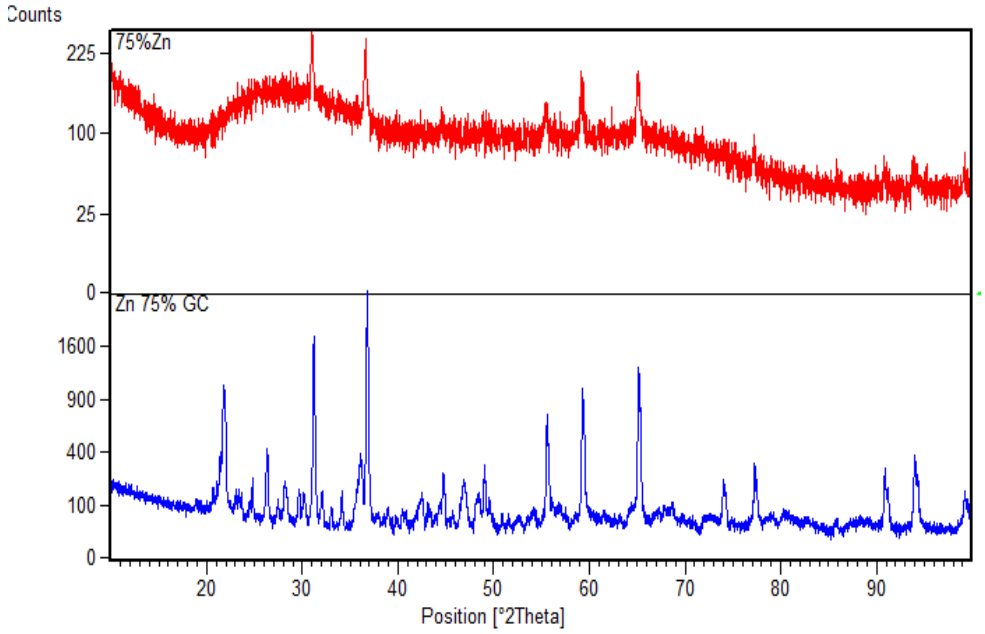


**Figure 3.2.6**: Comparison of X-ray powder diffraction patterns between LG26 Zn75% glass and LG26 Zn75% glass-ceramic.

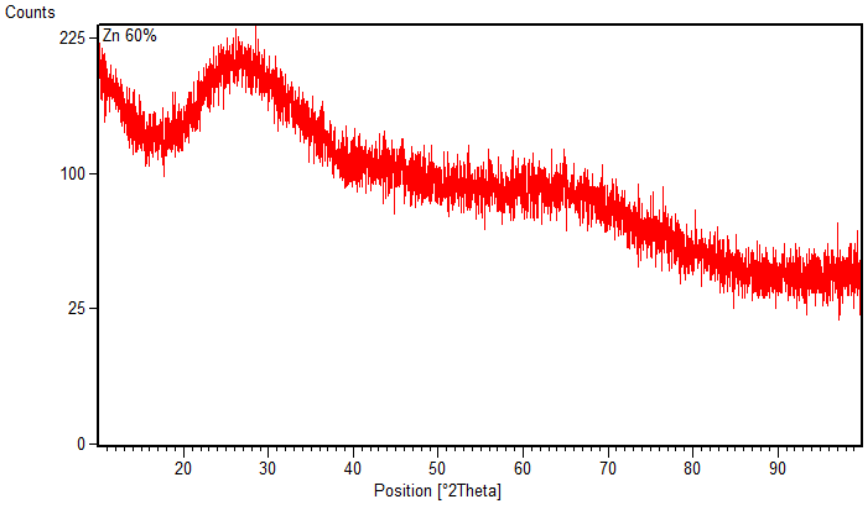


**Figure 3.2.7**: X-ray powder diffraction pattern of LG26 Zn60% glass.

X-ray diffraction was conducted in both coarse and fine particles of 60 and 75% substituted crystallized glasses. Figures 3.2.8 and 3.2.9 show that the particle size affected slightly the X-ray diffraction patterns. It was noticed, that coarse particle glass ceramic powders exhibited slightly larger amount of peaks especially smaller peaks compared to the fine particle glass ceramic powders. This suggests that some

other very minor phases were present in the coarse powders and as the differences were very small it was assumed that the same main crystalline phases were present in both coarse and fine glass ceramic powders.

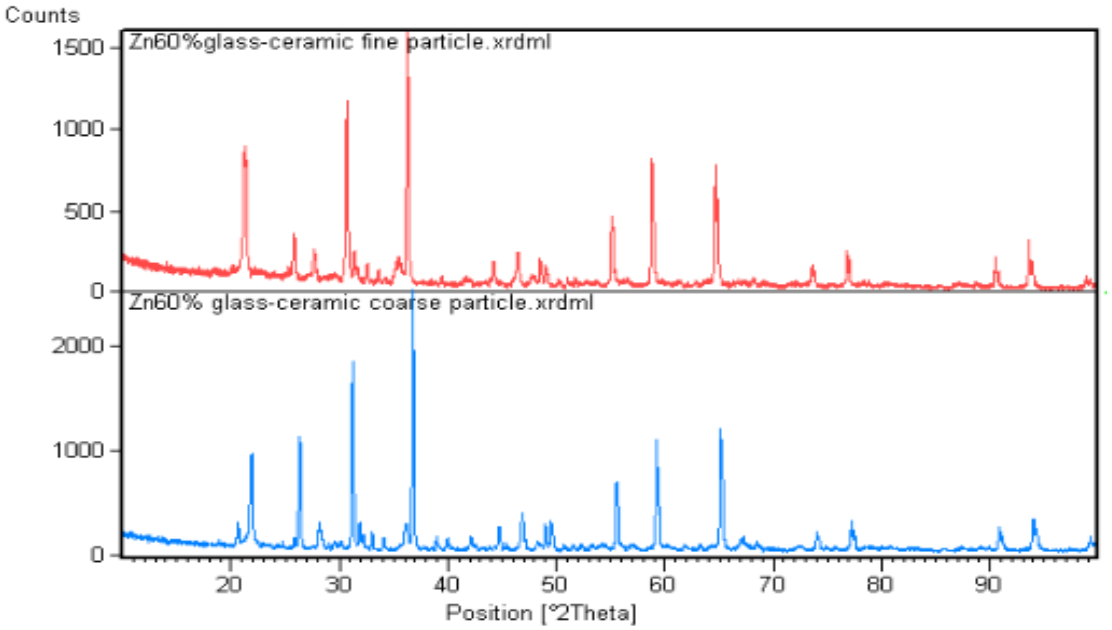


**Figure 3.2.8**: Comparison of X-ray powder diffraction patterns between LG26 60%Zn glass ceramics formed using coarse and fine glass powder.

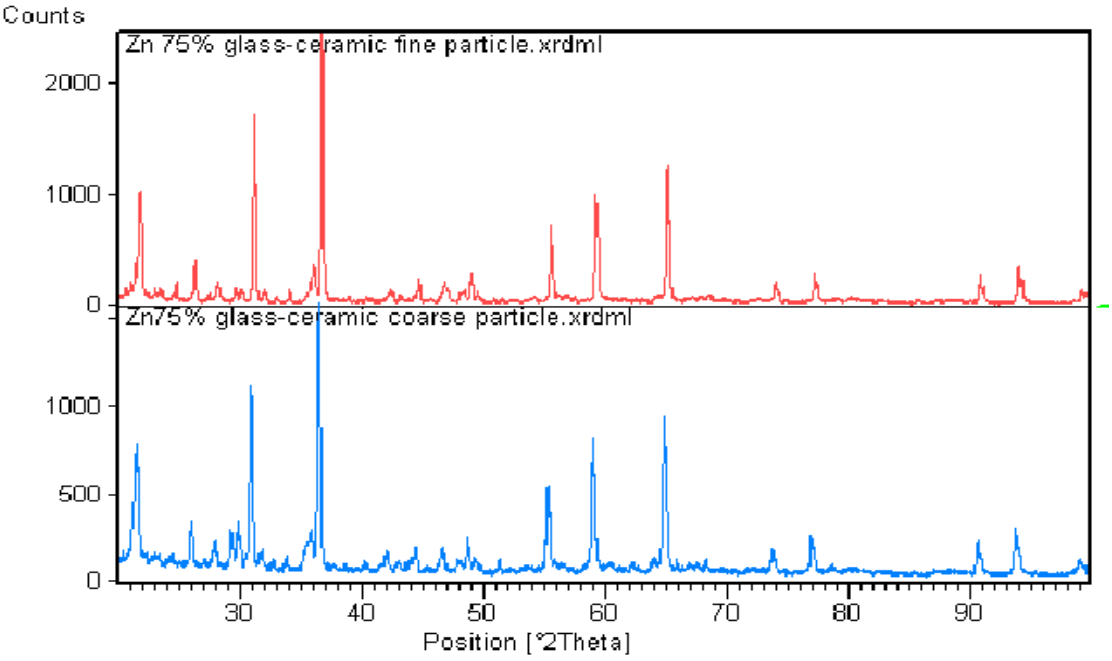


**Figure 3.2.9**: Comparison of X-ray powder diffraction patterns between LG26

75%Zn glass ceramics formed using coarse and fine glass powder.

Figure 3.2.10 shows the X-ray powder diffraction pattern of zinc containing glass-ceramics and 100%Ca containing glass-ceramic heat treated at 1100$^{o}$C with 1 hour hold. It is clear, that with zinc substitution subtle changes in the X-ray patterns occur. It is particularly clear, that the peaks related with the presence of fluorapatite gradually disappeared with substitution, whereas new peaks appeared slowly or some other peaks shifted. There seems to be a consistent tendency of the glasses with Zn substitution to form a Zn and Al rich phase that may result in Al not being available to form a Si and Al rich phase (lack of mullite). Since crystallization is very slow in this system and we heat treated all the glasses for the same period of time, it seems that a large amount of glass in 75% Zn substituted sample remains amorphous. Due to the lack of Al, fluorine does not form linkages with aluminium and it seems that remains as $ZnF_2$ in the amorphous glass. This however is a speculation as we do not have a clear evidence of any fluorine containing crystalline phase in the X-ray diffraction pattern of 75% Zn substituted glass ceramic.

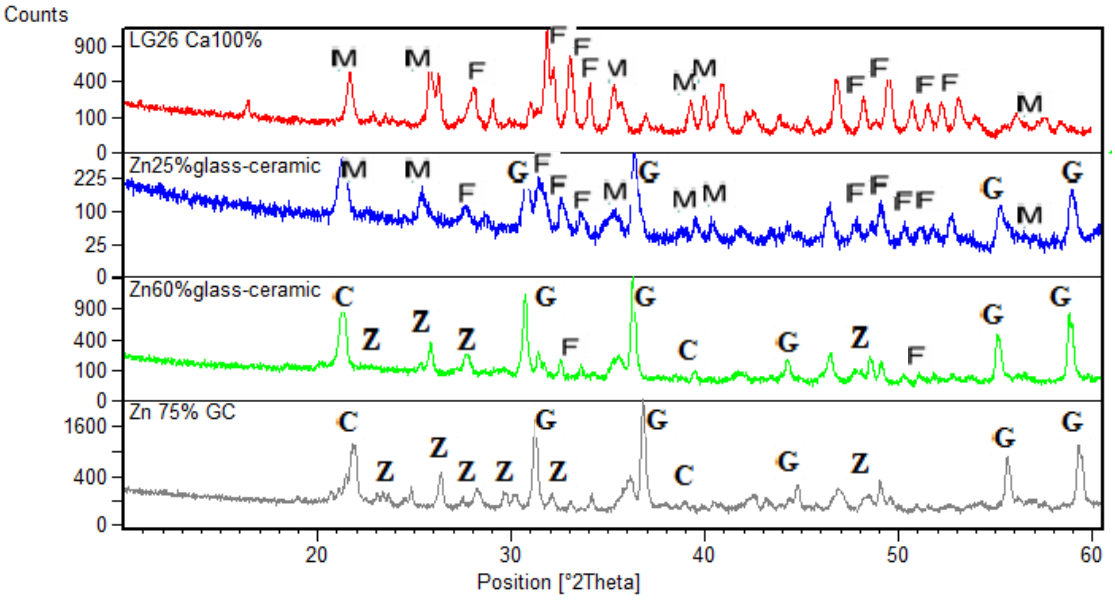


**Figure 3.2.10**: X-ray powder diffraction patterns of heat treated zinc substituted glasses (fine powder). F = Fluorapatite, M = Mullite, G= Gahnite, C= Cristobalite. Z= Calcium Zinc Phosphate.

Gahnite ($ZnAl_2O_4$) is widely used as ceramic, electronic and catalytic material. It can be synthesized by using conventional ceramic processing techniques, sol-gel method, coprecipitation method or alumina impregnating method following calcinations at relatively high temperatures (800-1000$^oC$). In addition, gahnite is characterized by its prominent performance such as high melting temperature (1950$^oC$), low thermal expansion coefficient ($5.5 \times 10^{-6}/^oC$, 25-1000 $^oC$) as well as high thermal stability and good resistance to acids and basicity [96]. It is therefore, worth mentioning that this new phase brings new characteristics to the glass ceramics under study and possibly opens new avenues for applications to explore.

### 3.2.1.2 XRD study of magnesium substituted glass-ceramics

In order to understand better the effect of the size of the cation in the crystalline structure of glasses, another glass composition was used as comparison based on magnesium substitution. Magnesium is slightly larger than zinc (Table 3.2.2) but seems to have a similar behavior in the glass network since some of the phenomena described above appeared also in Mg substituted glasses [97，98].

**Table.3.2.2**: Atomic number, weight and radius for calcium, magnesium and zinc.

| Elements | Atomic number | Atomic Weight (g) | Atomic radius (pm) |
|---|---|---|---|
| Ca | 20 | 40.078 | 197 |
| Mg | 12 | 24.3050 | 160 |
| Zn | 30 | 65.38 | 134 |

**Table 3.2.3**: Crystal phases in magnesium substituted glass-ceramics

| Glass | Crystal phases | | | |
|---|---|---|---|---|
| LG26(100%Ca) | $Ca_5(PO_4)_3F$ | x | $Al_6Si_2O_{13}$ | $AlPO_4$ |
| LG26Mg1(25%Mg) | $Ca_5(PO_4)_3F$ | $Mg_2PO_4F$ | $Al_6Si_2O_{13}$ | $AlPO_4$ |
| LG26Mg2(50%Mg) | $Ca_5(PO_4)_3F$ | $Mg_2PO_4F$ | $Al_6Si_2O_{13}$ | $AlPO_4$ |
| LG26Mg3(75%Mg) | x | $Mg_2PO_4F$ | $Al_6Si_2O_{13}$ | $AlPO_4$ |
| LG26Mg(100%Mg) | x | $Mg_2PO_4F$ | $Al_6Si_2O_{13}$ | $AlPO_4$ |

Table 3.2.3 presents the crystal phases formed when magnesium is substituted for calcium. It is clear, that fluorapatite does not form in 75 and 100% Mg substituted glass-ceramics, whereas Wagnerite appeared in all substituted glass-ceramics. Mullite formed in all substituted glass ceramics as did a minor aluminium phosphate phase. Figure 3.2.11 shows the X-ray powder diffraction patterns of all substituted glass ceramics and the calcium base glass-ceramic.

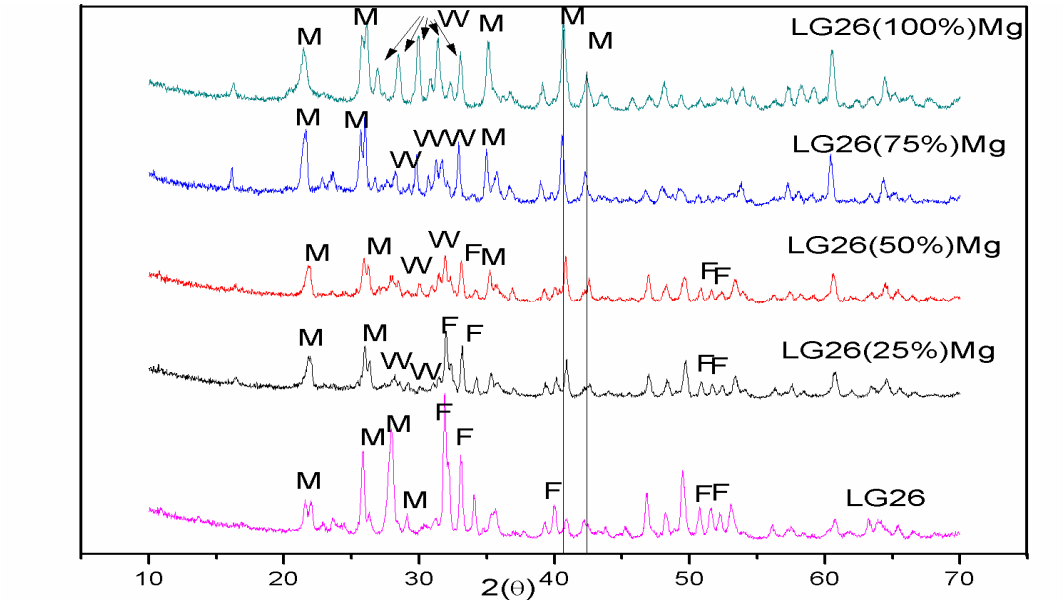


**Figure 3.2.11**: X-ray powder diffraction patterns of heat treated Mg substituted glasses. F = Fluorapatite, M = Mullite, W = Wagnerite. [97]

### 3.2.2 Density of Zinc Substituted Glass-Ceramics

Figure 3.2.2.1 shows the measured density of zinc substituted glass ceramics. It is clear, that the density for glass ceramics is increased with zinc substitution from 2.88 g/cm3 for LG26 ($4.5SiO_2$-$3Al_2O_3$-$1.5P_2O_5$-3CaO-$2CaF_2$) to 3.17 g/cm3 for LG26 75%Zn ($4.5SiO_2$-$3Al_2O_3$-$1.5P_2O_5$-3ZnO-$0.75ZnF_2$-$1.25CaF_2$). It is observed, that there is a linear relationship between the density and zinc molar content. In addition, in this case the density depends on the amount of phases formed in glass-ceramics.

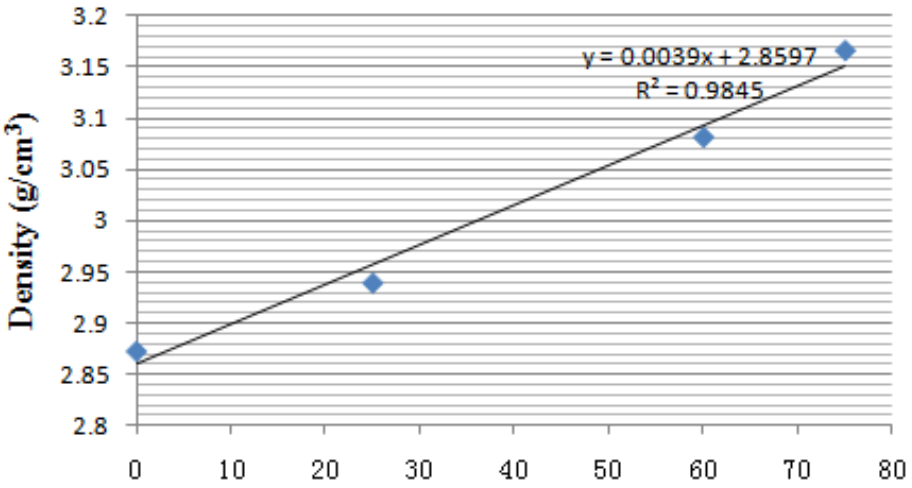


**Figure 3.2.2.1**: Density of zinc containing glass-ceramics.

The measured density values for glass ceramics are increased with increasing the molar content of zinc from 2.88 g/cm$^3$ of LG26 100%Ca containing glass ceramic to 3.17 g/cm$^3$ of LG26 75%Zn containing glass ceramic, shown in Figure 3.2.2.1. This happens because the density depends on the type of phases as well as the amount of the each phase formed in the glass ceramics. For instance, it has been calculated from the XRD reference that the density of crystal phases such as Ca-FAP (Ca5(PO4)3F) with reference code (00-015-0876) , Mullite (Al6Si2O13) with reference code (00-015-0776), Gahnite ($ZnAl_2O_4$) with reference code (00-005-0669), Calcium Zinc Phosphate ($CaZn_2(PO_4)_2$) (Ref.Code 00-020-0248) and Cristobalite ($SiO_2$) (Ref.Code 00-011-0695) are 3.15 g/cm$^3$, 3.00 g/cm$^3$, 4.62 g/cm$^3$, 3.9 g/cm$^3$, 2.27 g/cm$^3$ respectively [99]. Consequently, it can be explained why the LG26 75%Zn substituted

glass ceramic has the highest density value while the LG26 100%Ca substituted glass ceramic has the lowest value. According to the Table 3.2.1, it is observed that the LG26 75%Zn substituted glass ceramic consists of 3 crystal phases, Gahnite, Calcium Zinc Phosphate and Cristobalite while the LG26 100%Ca substituted glass ceramic consists of Ca-FAP, Mullite and $AlPO_4$. It is clear that the sum in the first case is much bigger than in the second.

### 3.2.3 FTIR studies of Zn substituted Glass-ceramics

In order to investigate the structure changes after the crystallization, all the zinc containing glasses were heated up to 1100$^{o}$C and hold 1 hour, then furnace cooled to room temperature, and characterized by FTIR in the wavenumber range of 4000-400cm$^{-1}$. In all FTIR spectra four main bands are observed: (1) The most intense absorption bands at 1120 and 1050 cm$^{-1}$ are due to the asymmetric stretching vibration(P-O, $v_3$) of phosphate tetrahedra with 4 NBOs ($PO_4$), and the absorption peak at 963 cm$^{-1}$ due to the symmetric stretching of phosphate group ($v_1$). (2) The peak situated at 472 cm$^{-1}$ is due to $v_2$ phosphate bending vibrations and is shifted to higher wavenumbers at 500 cm$^{-1}$ with zinc substitution suggesting higher degree of bond condensation. (3) It is obvious that the P-O peak in the original 100% Ca containing glass ceramic are two bonds (603 and 566 cm$^{-1}$) that correspond to the O-P-O bending of phosphate groups ($v_4$) and are characteristic of an apatite crystalline phase. (4) Al-O (AlO4) bonds are found to be present at 730 cm$^{-1}$ [100, 101]. It is indicated in the literature [102] that the gahnite phase is characterized at 660 cm$^{-1}$.

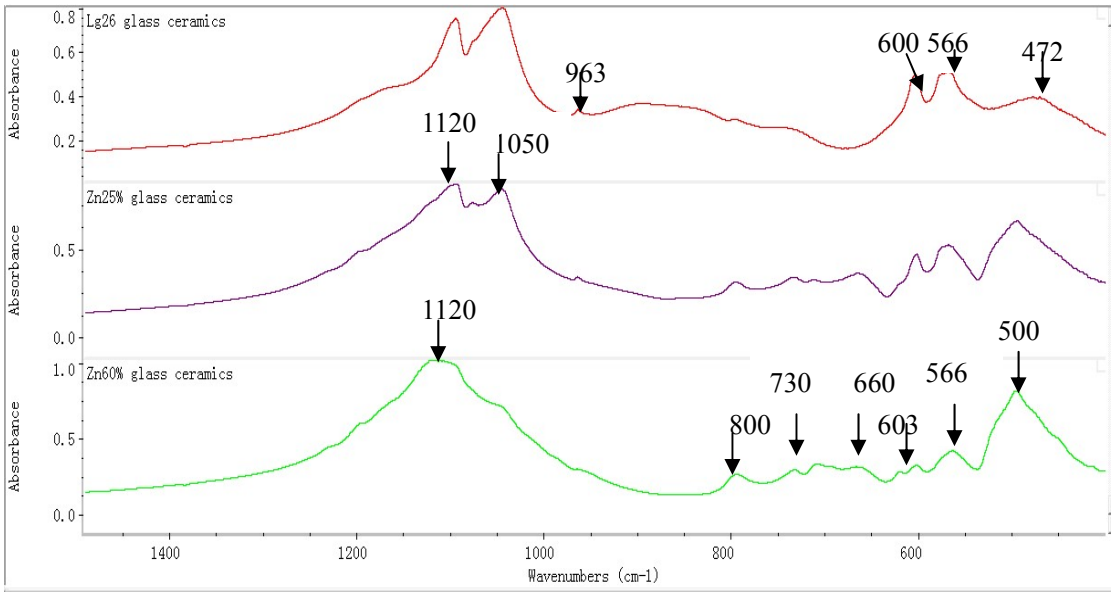


**Figure 3.2.3.1**: FTIR spectra of all zinc substituted glass-ceramics.

**Table 3.2.4:** Description of FTIR spectra for zinc substituted glass-ceramics

| *Wavenumber ($cm^{-1}$)* | ***LG26 100%Ca glass-ceramics*** | ***LG26 25%Zn glass-ceramics*** | ***LG26 60%Zn glass-ceramics*** | ***Description*** |
|---|---|---|---|---|
| | 472 | 500 | 500 | $v_2$ phosphate bending vibrations |
| | 600 | 600 | 566 , 603 | O-P-O bending of phosphate groups ($v_4$) |
| | 660 | 660 | 660 | Al-O stretching vibration of the structure of the gahnite phase [102] |
| | 730 | 730 | 730 | Al-O ($AlO_4$) bonds |
| | 1050, 1120 | 1050, 1120 | 1120 | The asymmetric stretching vibration(P-O,$v_3$) of phosphate tetrahedra with 4 NBOs ($PO_4$) [100,101] |

The XRD results confirm the formation of fluorapatite in the crystallized 100%Ca

containing glasses. When the zinc content (60%Zn) is more than that of calcium, a reduction in the absorbance intensity for both peaks (603 and 566 $cm^{-1}$) are detected in the FTIR spectra of zinc containing glass-ceramics, implying a decreasing preference of Ca-FAP formation proved by XRD study as well. In the literature the peak at 660 $cm^{-1}$ is assigned to Al-O (four-fold coordination) stretching vibration of the structure of the gahnite phase and we can find it in 25 and 60% Zn glass ceramics.

### 3.2.4 Raman analysis of zinc substituted glasses

There are a number of reviews of Raman scattering in solids and the author is referred to these works [103, 104]. A concise summary of the theory is presented below. An isolated $[PO_4]^{3-}$ has $T_d$ symmetry and four normal modes of vibration: $A_1$ ($v_1$) =955$cm^{-1}$, E ($v_2$) = 425$cm^{-1}$, $T_2$ ($v_3$) =1043$cm^{-1}$, and $T_2$ ($v_4$) =578$cm^{-1}$, where the species E vibrations are doubly degenerate and $T_2$ vibrations are triply degenerate [105]. The effect of the crystal field of the fluorapatite lattice on internal vibrational modes may be understood by considering the phosphate site symmetry. The $T_d$ symmetry of a free tetrahedral $[PO_4]^{3-}$ ion is reduced to Cs in the crystal lattice. This symmetry change removes some of the degeneracies of the vibrational wave functions which would have characterized free $[PO_4]^{3-}$ ion. In Table 3.2.5 is demonstrated, that the gahnite phase appears in 25, 60 and 75% zinc substituted glass-ceramics, and the related regions are 410-420 and 600-700$cm^{-1}$ [106]. The peak at 1120 $cm^{-1}$ is probably due to P-O stretching in units that may resemble three-dimensionally interconnected structure of $AlPO_4$ [107]. Generally, all glass ceramics exhibit similar Raman peaks and on of the main differences is differences in the intensity of peaks. Especially in the case of 75% Zn substituted glass-ceramic where most peaks are quite broad and not sharp. This probably reflects the lower degree of crystallinity of the sample compared to the rest of samples. Finally, the peaks at 271 and 223 $cm^{-1}$ present in the Raman spectra of 25, 60 and 75% Zn substituted glass ceramics can be associated with the $SiO_2$ cristobalite phase detected in the XRD diffractogramms as well.

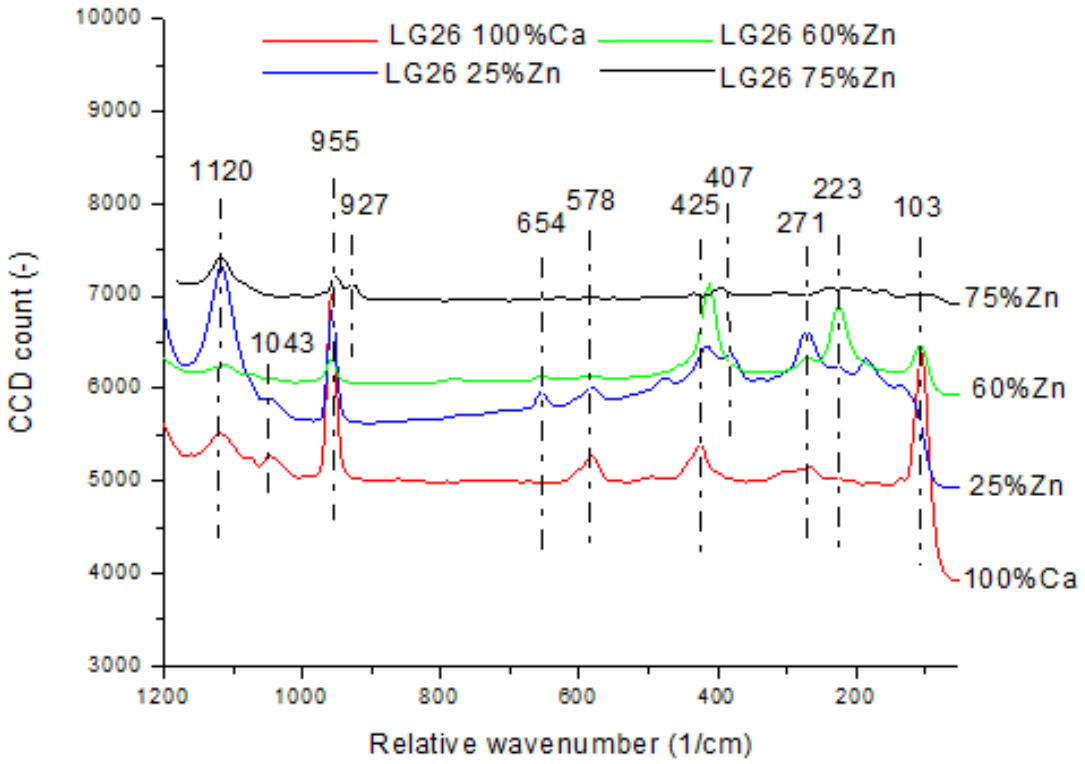


**Figure 3.2.3.2**: Raman spectrum of zinc substituted glass-ceramics.

**Table 3.2.5:** Assignment of Raman peaks in fluorapatite from the literature.

| *Wavenumber (cm$^{-1}$)* | *Description* |
|---|---|
| 420 | $v_2$ ($PO_4$) bending vibration |
| 567 | $v_4$ ( $PO_4$ ) bending vibration |
| 938 | $v_1$ ($PO_4$) symmetric stretching vibration |
| 1017 | $v_3$ ($PO_4$) anti-symmetric stretching vibration [103-106] |

**Table 3.2.6:** Analysis of Raman spectra for zinc substituted glass-ceramics

| *Wavenumber* | *LG26 100%Ca* | *LG26 25%Zn* | *LG26 60%Zn* | *LG26 75%Zn* | *Description*[100-103] |
|---|---|---|---|---|---|
| 578 | 578 | ---- | ---- | $v_4$ ( $PO_4$ ) bending vibrations | |

| | | | | |
|---|---|---|---|---|
| 1043 | 1043 | ---- | ---- | $\nu_3$ ($PO_4$) anti-symmetric stretching vibrations |
| 425 | 425, 407 | 420 | 415 | $\nu_2$ ($PO_4$) bending vibrations |
| 955 | 955 | 955 | 955, 927 | $\nu_1$ ($PO_4$) symmetric stretching vibrations |
| 1120 | 1120 | 1120 | 1120 | P-O stretching vibrations in $AlPO_4$ [107] |
| ---- | 654, 407 | 654, 407 | 654, 407 | Gahnite ($ZnAl_2O_4$) |
| ---- | 271 | 223 | 223 | Cristobilte |

### 3.3 ESEM and EDX studies of Mg and Zn substituted glass-ceramics

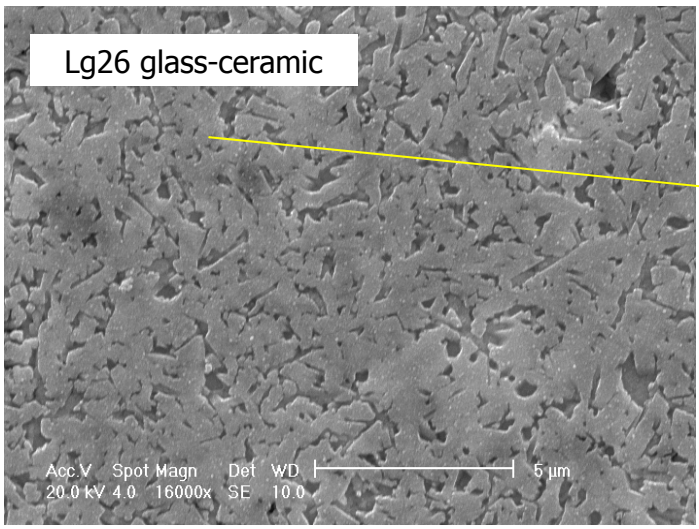


| Element | Weight% | Atomic% |
|---|---|---|
| | | |
| O | 43.29 | 58.46 |
| F | 5.38 | 6.12 |
| Al | 15.82 | 12.67 |
| Si | 10.35 | 7.96 |
| P | 7.78 | 5.43 |
| Ca | 17.37 | 9.37 |
| | | |
| Totals | 100 | |

**Fluorapatite, Mullite and a small amount of $AlPO_4$**

**Figure 3.3.1**: ESEM and EDX analysis of LG26 100%C

Figure 3.3.1 shows an ESEM micrograph and EDX analysis for the calcium base

glass ceramic. The surface in the micrograph above exhibits one phase morphology: needle-like (mullite and fluorapatite).

Figures 3.3.2 to 3.3.5 show the microstructure and morphology of different magnesium substituted for calcium glass-ceramics.

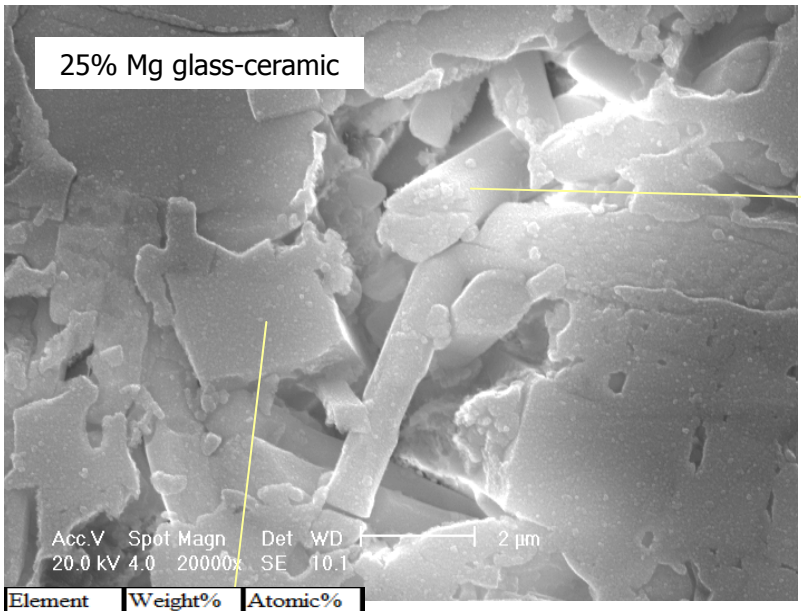


| Element | Weight% | Atomic% |
|---|---|---|
| | | |
| C | 14.48 | 23.35 |
| O | 39.06 | 47.27 |
| F | 6.63 | 6.76 |
| Mg | 0.35 | 0.28 |
| Al | 3.07 | 2.2 |
| Si | 4.84 | 3.33 |
| P | 10.96 | 6.85 |
| Ca | 20.62 | 9.96 |
| | | |
| Totals | 100 | |

**Fluorapatite**

| Element | Weight% | Atomic% |
|---|---|---|
| | | |
| C | 14.49 | 21.9 |
| O | 45.66 | 51.8 |
| F | 2.79 | 2.66 |
| Mg | 0.72 | 0.54 |
| Al | 19.4 | 13.05 |
| Si | 10.35 | 6.69 |
| P | 2.81 | 1.65 |
| Ca | 3.78 | 1.71 |
| | | |
| Totals | 100 | |

**Mullite**

**Figure 3.3.2**: ESEM and EDX analysis of LG26 25%Mg glass-ceramic.

From Figure 3.3.2 is clear, that 25mol% magnesium substituted glass-ceramic exhibits two different morphologies: plate-like crystals assigned to mullite and needle-like crystals with hexagonal profile assigned to fluorapatite.

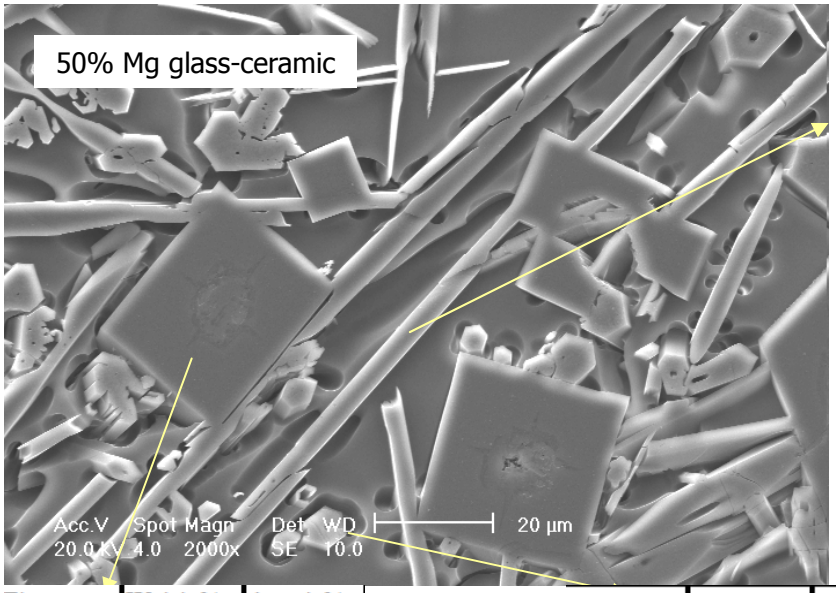


| Element | Weight% | Atomic% |
|---|---|---|
| | | |
| C | 15.9 | 24.08 |
| O | 33.64 | 38.24 |
| F | 12.73 | 12.19 |
| Mg | 21.78 | 16.3 |
| P | 14.67 | 8.61 |
| Ca | 1.27 | 0.58 |
| | | |
| Totals | 100 | |

**Wagnerite**

| Element | Weight% | Atomic% |
|---|---|---|
| | | |
| C | 16.64 | 24.76 |
| O | 44.65 | 49.87 |
| Mg | 0.75 | 0.55 |
| Al | 28.09 | 18.6 |
| Si | 9.11 | 5.8 |
| P | 0.61 | 0.35 |
| Ca | 0.14 | 0.06 |
| | | |
| Totals | 100 | |

**Mullite**

| Element | Weight% | Atomic% |
|---|---|---|
| | | |
| C | 14.28 | 23.28 |
| O | 29.53 | 36.15 |
| F | 19.18 | 19.78 |
| Mg | 1.02 | 0.82 |
| Al | 1.93 | 1.4 |
| Si | 1.77 | 1.23 |
| P | 10.75 | 6.8 |
| Ca | 21.54 | 10.53 |
| | | |
| Totals | 100 | |

**Fluorapatite**

**Figure 3.3.3**: ESEM and EDX analysis of LG26 50%Mg glass-ceramic.

Similarly from Figure 3.3.3 is shown that 50mol% magnesium substituted glass-ceramic exhibits two different phase morphologies: plate-like crystals assigned to mullite and needle-like crystals assigned to both wagnerite and fluorapatite.

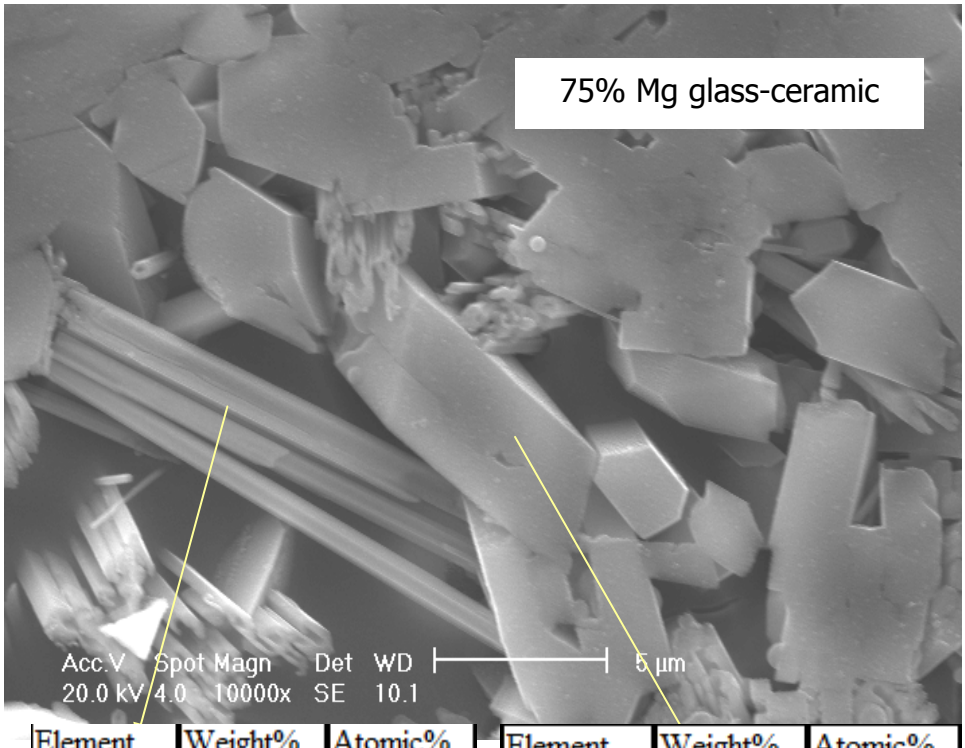


| Element | Weight% | Atomic% |
|---|---|---|
| | | |
| C | 15.49 | 23.37 |
| O | 36.89 | 41.78 |
| F | 10.5 | 10.01 |
| Mg | 13.9 | 10.36 |
| Al | 9.33 | 6.26 |
| Si | 3.55 | 2.29 |
| P | 9.42 | 5.51 |
| Ca | 0.93 | 0.42 |
| | | |
| Totals | 100 | |

**Wagnerite phase**

| Element | Weight% | Atomic% |
|---|---|---|
| | | |
| C | 17.31 | 26.07 |
| O | 42.86 | 48.44 |
| F | 5.54 | 5.27 |
| Mg | 1.98 | 1.48 |
| Al | 6.69 | 4.49 |
| Si | 8.79 | 5.66 |
| P | 7.54 | 4.4 |
| Ca | 9.29 | 4.19 |
| | | |
| Totals | 100 | |

**Mullite and Fluorapatite phases**

**Figure 3.3.4**: ESEM and EDX analysis of LG26 75%Mg glass-ceramic.

The ESEM micrographs and EDX presented in Figure 3.3.4 suggested that 75mol% magnesium substituted glass-ceramic exhibited also two different phase morphologies: plate-like crystals assigned to mullite and, needle-like crystals assigned to wagnerite.

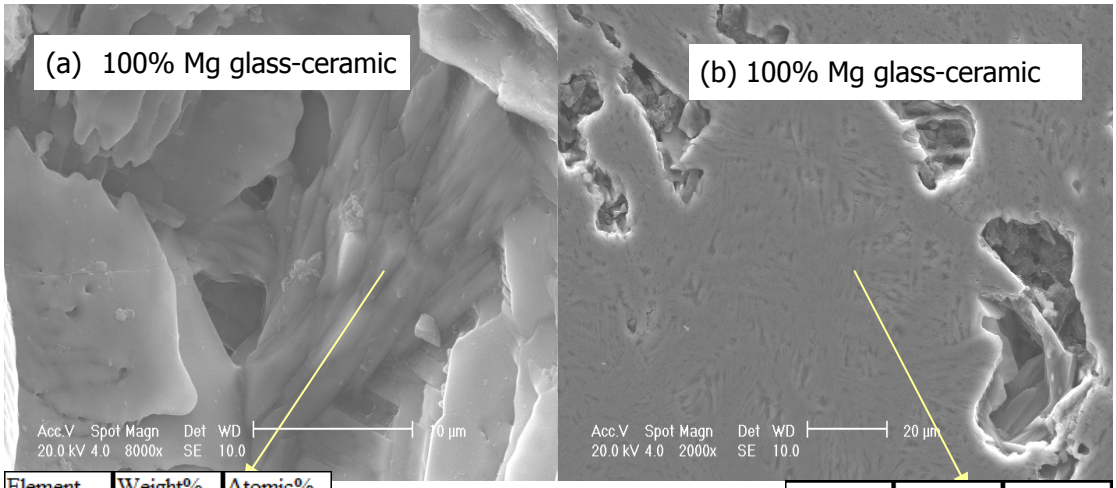


| Element | Weight% | Atomic% |
|---|---|---|
| | | |
| C | 17.9 | 25.41 |
| O | 43.2 | 46.05 |
| F | 13.9 | 12.48 |
| Mg | 10.87 | 7.62 |
| Al | 5.55 | 3.51 |
| Si | 3.61 | 2.19 |
| P | 4.97 | 2.74 |
| | | |
| Totals | 100 | |

**Mixed Phases**

| Element | Weight% | Atomic% |
|---|---|---|
| | | |
| C | 13.23 | 20.22 |
| O | 40.62 | 46.6 |
| F | 6.6 | 6.37 |
| Mg | 9.89 | 7.46 |
| Al | 13.56 | 9.23 |
| Si | 9.34 | 6.1 |
| P | 6.77 | 4.01 |
| | | |
| Totals | 100 | |

**Figure 3.3.5**: ESEM and EDX analysis of LG26 100%Mg glass-ceramic.

On the other hand, in the case of 100% magnesium glass ceramic ESEM micrographs and EDX analysis (Figure 3.3.5) suggested that the mullite and wagnerite phases were well mixed and it was difficult to distinguish between them. Etching of the surface by HF showed that Wagnerite appeared also needle-like (Figure 3.3.5 (b)).

Figures 3.3.6 to 3.3.8 show the microstructure and morphology of different zinc substituted glass-ceramics. Figure 3.3.6 represents the ESEM and EDX analysis for 25% Zn substituted glass ceramic. The etched surface of the glass ceramic seems to be very similar to the etched surfaces observed in previous work where needle-like fluorapatite was present [98]. EDX analysis however showed that gahnite which is a new phase formed when Zn was substituted for Ca seems to be also needle-like, however this is not very clear from the micrograph as needle like crystals are also due to the presence of fluorapatite and mullite. It is worth noticing that the needle-like crystals have a different profile which is not hexagonal as the fluorapatite crystals.

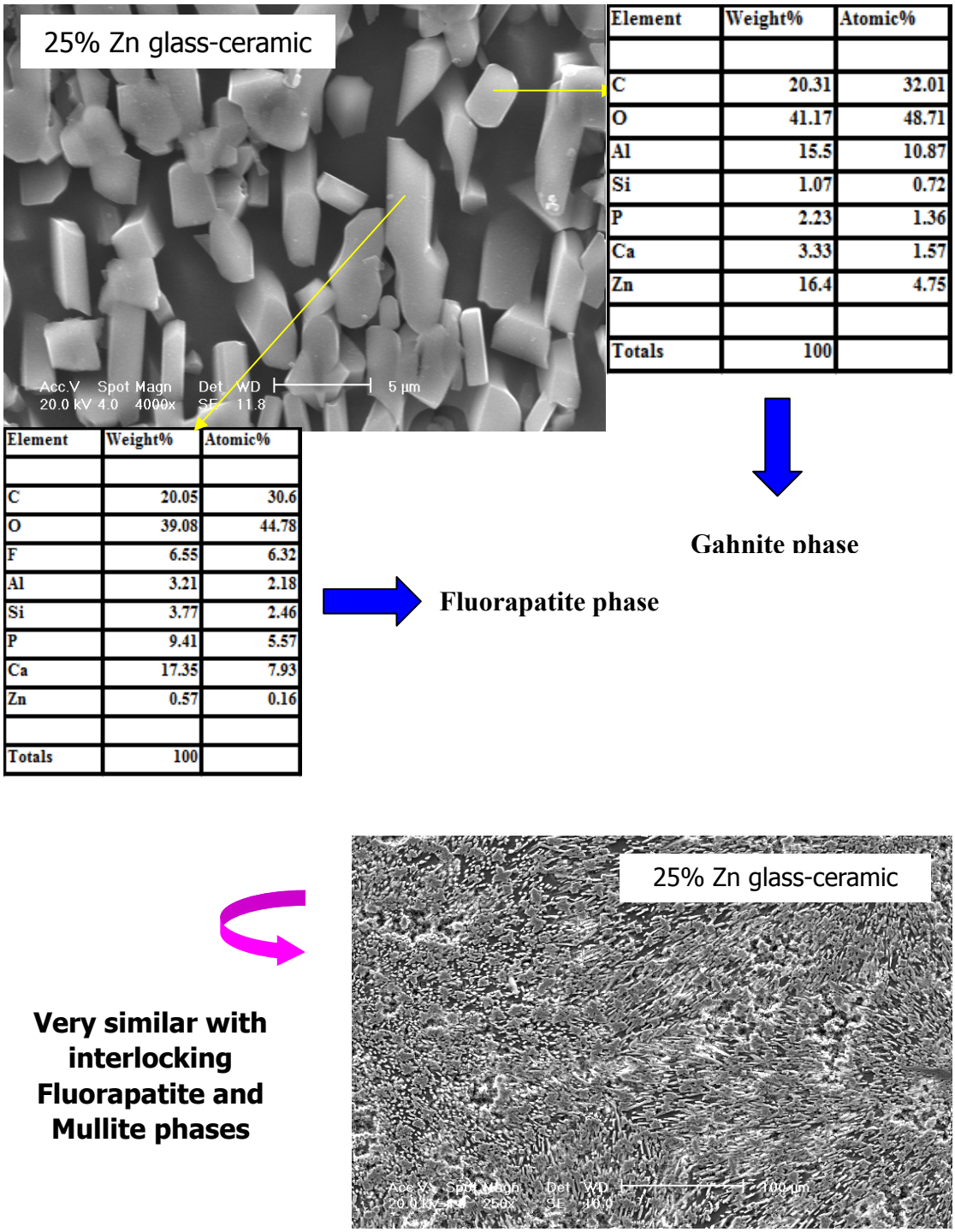


**Figure 3.3.6**: ESEM and EDX analysis of LG26 25%Zn glass-ceramic.

Figure 3.3.7 shows the ESEM and EDX analysis of 60% Zn substituted glass ceramic. It is clear here that fluorapatite is still present as a needle-like phase, whereas gahnite has taken up a polygonal particle morphology.

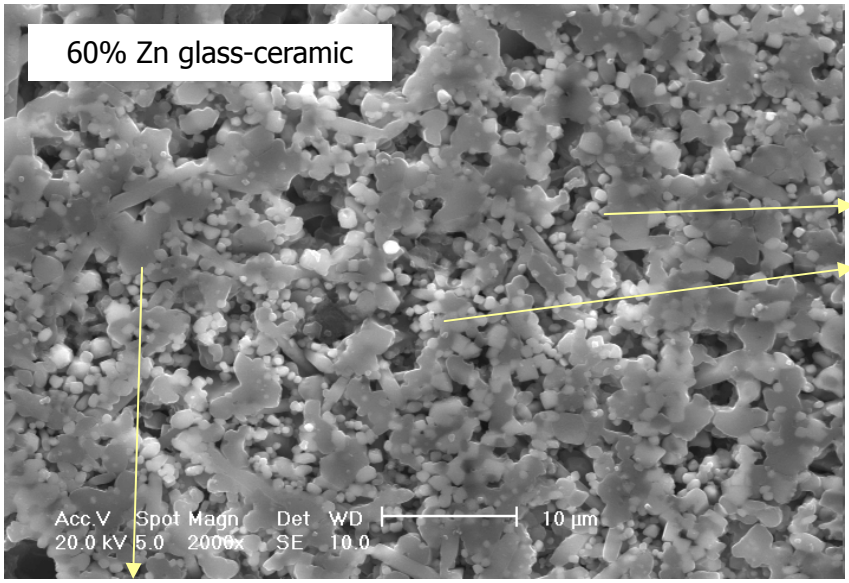


| Element | Weight% | Atomic% |
|---|---|---|
| C | 22.03 | 36.54 |
| O | 31.59 | 39.34 |
| F | 1.32 | 1.38 |
| Al | 13.23 | 9.77 |
| Si | 6.3 | 4.47 |
| P | 0.86 | 0.55 |
| Ca | 2.15 | 1.07 |
| Zn | 22.53 | 6.87 |
| Totals | 100 | |

| Element | Weight% | Atomic% |
|---|---|---|
| C | 20.27 | 34.41 |
| O | 30.39 | 38.72 |
| F | 2.64 | 2.83 |
| Al | 15.82 | 11.95 |
| Si | 4.05 | 2.94 |
| P | 0.25 | 0.16 |
| Ca | 3.51 | 1.78 |
| Zn | 23.07 | 7.2 |
| Totals | 100 | |

Gahnite and Cristobalite phases

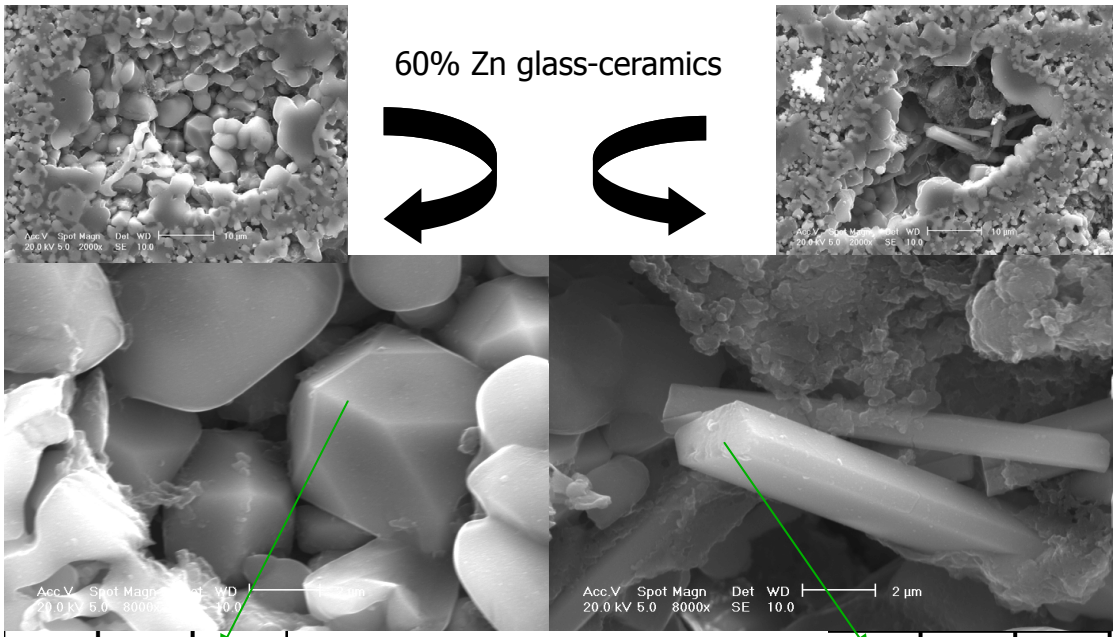


| | | |
|---|---|---|
| C | 21.16 | 34.54 |
| O | 35.39 | 43.37 |
| F | 0.95 | 0.98 |
| Al | 17.26 | 12.54 |
| Si | 2.26 | 1.58 |
| P | 0.14 | 0.09 |
| Ca | 0.34 | 0.17 |
| Zn | 22.51 | 6.75 |
| Totals | 100 | |

**Fluorapatite Phase**

**Gahnite Phase**

**Zn/Al=1/2**

| | | |
|---|---|---|
| C | 23.15 | 34.74 |
| O | 38.58 | 43.46 |
| F | 6.07 | 5.76 |
| Al | 0.5 | 0.34 |
| Si | 3.05 | 1.96 |
| P | 9.26 | 5.39 |
| Ca | 17.37 | 7.81 |
| Zn | 2.03 | 0.56 |
| Totals | 100 | |

**Figure 3.3.7**: ESEM and EDX analysis of LG26 60%Zn glass-ceramic.

Figure 3.3.8 shows the ESEM and EDX analysis of 75% Zn substituted glass ceramic. It can be observed, that the morphology of the crystal phases present is quite different to the morphology observed for the other glass ceramics above. It seems that the crystal phases can be seen in a matrix of amorphous glass something that was also suggested by the XRD and the Raman spectroscopy data. The EDX measurements show clearly the presence of fluorine although no fluorine containing crystal phase was identified in the glass ceramic. This leads to the conclusion that fluorine must have remained in the amorphous glass. Unfortunately, it can be only a speculation that fluorine must be as $ZnF_2$ in the glass as there is no other indication from the data presented here. As explained in the XRD analysis section, aluminium seems to link with Zn to form gahnite and therefore lack of aluminium would result in fluorine being available within the amorphous glass network. Another possibility could be that fluorine forms Si-F linkages resulting to the formation of $SiF_4$ and therefore some loss of weight at high temperatures as observed in the TGA results. Further more systematic study could possibly give an answer to the above speculation.


| Element | Weight% | Atomic% |
|---|---|---|
| | | |
| C | 25.01 | 36.52 |
| O | 41.33 | 45.3 |
| F | 1.61 | 1.48 |
| Al | 4.31 | 2.8 |
| Si | 16.12 | 10.07 |
| P | 1.28 | 0.72 |
| Ca | 1.94 | 0.85 |
| Zn | 8.4 | 2.25 |
| | | |
| Totals | 100 | |

**Cristobalite ($SiO_2$) phase**

| Element | Weight% | Atomic% |
|---|---|---|
| | | |
| C | 20.49 | 32.22 |
| O | 29.63 | 34.98 |
| F | 16.26 | 16.17 |
| Al | 8.25 | 5.78 |
| Si | 3.16 | 2.12 |
| P | 2.71 | 1.65 |
| Ca | 7.93 | 3.74 |
| Zn | 11.56 | 3.34 |
| | | |
| Totals | 100 | |

**Gahnite phase**

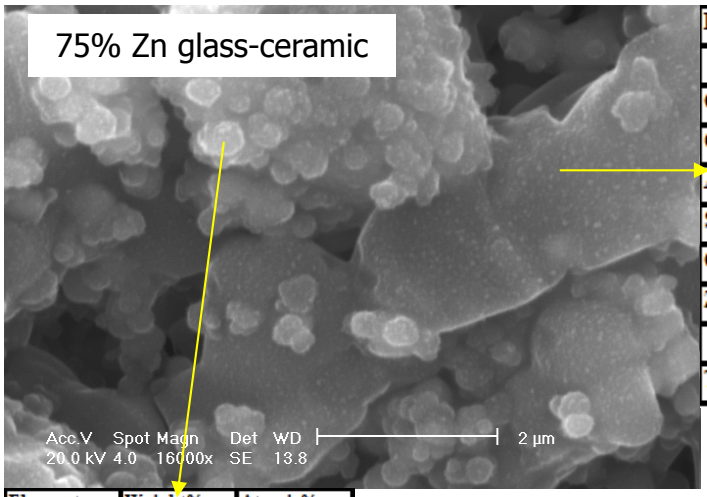


| Element | Weight% | Atomic% |
|---|---|---|
| | | |
| C | 24.53 | 36.63 |
| O | 39.91 | 44.74 |
| Al | 5.41 | 3.59 |
| Si | 18.39 | 11.74 |
| Ca | 0.38 | 0.17 |
| Zn | 11.39 | 3.13 |
| | | |
| Totals | 100 | |

**Cristobalite ($SiO_2$) phase**

| Element | Weight% | Atomic% |
|---|---|---|
| | | |
| C | 24.14 | 38.03 |
| O | 34.1 | 40.33 |
| F | 2.83 | 2.82 |
| Al | 13.17 | 9.24 |
| Si | 4.74 | 3.19 |
| P | 0.78 | 0.48 |
| Ca | 0.29 | 0.14 |
| Zn | 19.96 | 5.78 |
| | | |
| Totals | 100 | |

**Gahnite phase**

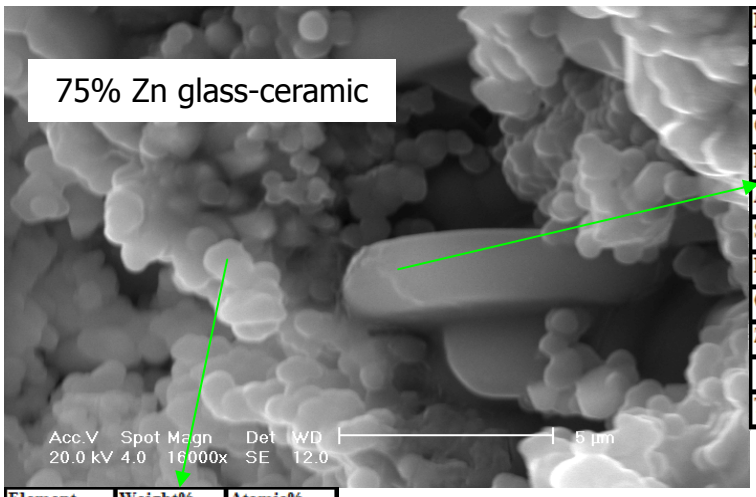


| Element | Weight% | Atomic% |
|---|---|---|
| | | |
| C | 19.31 | 33.91 |
| O | 26.19 | 34.53 |
| F | 10.99 | 12.2 |
| Al | 3.9 | 3.05 |
| Si | 5.55 | 4.17 |
| P | 2.19 | 1.49 |
| Ca | 1.8 | 0.95 |
| Zn | 30.08 | 9.71 |
| | | |
| Totals | 100 | |

| Element | Weight% | Atomic% |
|---|---|---|
| | | |
| C | 15.42 | 33.89 |
| O | 17.81 | 29.39 |
| F | 4.53 | 6.29 |
| Al | 3.38 | 3.31 |
| Si | 3.65 | 3.43 |
| P | 1.55 | 1.32 |
| Ca | 2.43 | 1.6 |
| Fe | 1.09 | 0.51 |
| Zn | 50.15 | 20.25 |
| | | |
| Totals | 100 | |

**Gahnite and Calcium Zinc Phosphate phase ($CaZn_2(PO_4)_2$)**

**Figure 3.3.8**: ESEM and EDX analysis of LG26 75%Zn glass-ceramic.

# CHAPTER 4: CONCLUSIONS

## 4. Conclusions

An original ionomer glass composition $4.5SiO_2$-$3Al_2O_3$-$1.5P_2O_5$-3CaO-$2CaF_2$ was used to make the glass by a melt-quench route at1450$^oC$. A series of zinc substituted glasses were produced by substituting Zn for Ca in 25mol% (LG26 25%Zn), 60mol% (LG26 60%Zn), 75mol% (LG26 75%Zn) and 100mol% (LG26 100%Zn). The frit glasses were milled and sieved to give fine particles (<45μm) and coarse particles (45μm-100μm). The characterization of glasses and glass ceramics included density measurements by a Helium Pycnometer and thermal analysis by DSC and TGA. FTIR and Raman spectroscopy was conducted in both glasses and glass ceramics. The crystal phases in glass ceramics were identified by X-ray diffraction. The morphology of the crystal phases was observed by ESEM and the identification of the crystals observed was achieved by EDX. The following conclusions can be drawn from the above work:

1. The density of zinc substituted glasses and glass-ceramics both increased with increasing zinc content. The oxygen density did not change significantly although FTIR spectroscopy did suggest an increase of bridging oxygens with zinc substitution.
2. The glass transition temperature decreased with zinc substitution whereas the crystallization temperature was affected by the particle size of the glasses and although crystallization was not recorded when coarse particles of glass were analyzed, the crystallization temperature when fine particles were used generally increased with substitution and above 60% only one crystallization temperature was recorded. Isothermal studies for the coarse glass particles were conducted in order to study the crystallization process that was thought to be very slow. The crystallization temperatures recorded had an increasing tendency with zinc substitution. The endothermic process observed at above

1200$^{o}$C during the DSC analysis may be associated with crystal dissolution. Crystal dissolution temperatures decreased with zinc substitution. It is worth noticing, that all the thermogravimetric analysis was conducted on fine powder glass samples and it was expected that if there was a weight loss this should be due to the larger surface area. It is suggested, that there is a small fluorine loss from the surface of the glasses due to possibly $SiF_4$ formation during heating. It is clear, that the zinc substituted glasses are different than the calcium base glass and therefore it is expected that the crystallization mechanism and phases formed should be also different.

**3.** The FTIR and Raman spectra are not conclusive. It was observed that, when Zn concentration increased, the position of both Si-O-Si stretching ($Q^3$) (1099cm$^{-1}$) and Si-O-[NBO] bands (980cm$^{-1}$) shifted towards higher values (1105cm$^{-1}$ and 985cm$^{-1}$, respectively), and the intensity of the band associated with Si-O-[NBO] generally decreased. The declination of the intensity of Si-O-[NBO] suggests that there was more Si-O-Si as well as bridging-oxygens formed in the glass network. The XRD results confirm the formation of fluorapatite in the crystallized 100%Ca containing glasses. When the zinc content (60%Zn) is more than that of calcium, a reduction in the absorbance intensity for both peaks (603 and 566 cm$^{-1}$) is observed in the FTIR spectra of zinc containing glass-ceramics, implying a decreasing preference of Ca-FAP formation proved by XRD study as well. In the literature the peak at 660 cm$^{-1}$ is assigned to Al-O (four-fold coordination) stretching vibration of the structure of the gahnite phase that was clearly observed in the spectra of 25 and 60% Zn glass ceramics. All glass ceramics exhibit similar Raman peaks with some differences in the intensity of specific bands. Especially in the case of 75% Zn substituted glass-ceramic where most peaks are quite broad and not sharp. This probably reflects the lower degree of crystallinity of the sample compared to the rest of materials. The presence of a $SiO_2$ cristobalite phase in 25, 60 and 75% Zn glass ceramics was identified by both Raman spectroscopy ( peaks at 271 and 223 cm$^{-1}$) X-ray diffraction.

4. Fluorapatite and mullite are present in the calcium base glass ceramics. However, new phases appeared with zinc substitution thought to be gahnite ($ZnAl_2O_4$) and calcium zinc phosphate ($CaZn_2(PO_4)_2$). It is particularly clear, that in the diffrcatogramms the peaks related with the presence of fluorapatite gradually disappeared with substitution, whereas new peaks appeared slowly or some other peaks shifted. There seems to be a consistent tendency of the glasses with Zn substitution to form a Zn and Al rich phase that may result in Al not being available to form a Si and Al rich phase (lack of mullite). Since crystallization is very slow in this system and all glasses were heat treated for the same period of time, it seems that a large amount of glass in 75% Zn substituted sample remains amorphous. Due to the lack of Al, fluorine does not form linkages with aluminium and it seems that remains as $ZnF_2$ in the amorphous glass. This however is a speculation as there is no clear evidence of any fluorine containing crystalline phase in the X-ray diffraction pattern of 75% Zn substituted glass ceramic.
5. The morphology of the crystal phases formed change with zinc and magnesium substitution as was observed by ESEM. For example, mullite in magnesium substituted glass-ceramics appears to be plate-like but in zinc substituted glass-ceramics mullite forms as a needle-like crystal phase. The gahnite phase appears as a polygonal particle (possibly octagonal) whereas the atomic ratio of Zn/Al in the crystal phase is ½ as estimated by EDX analysis.

# CHAPTER 5: FUTURE WORK

## 5. Future work

In the future, further work should be carried out in order to develop a complete understanding of the crystallization mechanism for zinc substituted glasses as well as the structure of both glasses and glass ceramics:

1. All zinc substituted glasses produced should be characterized by differential scanning calorimetry to obtain the optimum nucleation temperature and activation energy of fluorapatite formation which will be calculated by the Marrotta and Kissinger methods.
2. Multinuclear MAS-NMR study should be conducted in all zinc substituted glasses and glass ceramics in order to establish the main species present, whether the glasses are phase separated at high Zn contents, what is the local environment around a silicon atom or a fluorine atom etc. The latter will help particularly in the case of 75% Zn substituted glass and glass ceramic, where fluorine seem to be present in the amorphous glass and no sign of a fluorine containing crystal phase is present. Also, multinuclear MAS-NMR may help to develop an understanding of why Zn substituted glasses crystallize slowly and phase separate.

## 6. References


[1] A. Clifford, R. Hill, A. Rafferty, P. Mooney, D. Wood, B. Samuneva, S. Matusuya, J. Mater. Sci. Mater. Med. 12 (2001) 461.

[2] C. Jana, W. Holand, Silic. Ind. 56 (1991) 215.

[3] M. D. Snyder, B. R. Lang & M. E. Razzoog, "The efficacy of luting all-ceramics crowns with resin-modified glass ionomer cement", *American Dental Association*, vol. 134, pp. 609-612, 2003.

[4] A. D. Wilson and B. E. Kent, "Dental Cements: Decomposition of the Powder", *Journal of Dental Research*, pp. 7-13, 1970.

[5] A. D. Wilson and B. E. Kent, "A new translucent cement for dentistry", *British Dental Journal*, vol. 132, pp. 133-135, 1972.

[6] J. E. Shelby, "Introduction to Glass Science and Technology (RSC paperbacks)", The Royal Society of Chemistry, 1997.

[7] J. W. Nicholson, "Chemistry of glass-ionomer cements: a review", *Biomaterials*, vol 19, pp. 485-494, 1998

[8] A. D. Wilson, D. M. Groffman & A. T. Kuhn, *Biomaterials*, vol. 6, pp. 431-433, 1985.

[9] K. Stanton and R. Hill, "The role of fluorine in the devitrification of $SiO_2{\cdot}Al_2O_3{\cdot}P_2O_5{\cdot}CaO{\cdot}CaF_2$ glasses", *Journal of Materials Science*, vol. 35, pp. 1911–1916, 2000.

[10] C.M. Crowley, J. Doyle, M. R. Towler, R. G. Hill, and S. Hampshire, "The influence of capsule geometry and cement formulation on the apparent viscosity of dental cement", *Journal of Dentistry*, vol. 34, pp. 566-573, 2006.

[11] M. R. Towler, C. M. Crowley, and R. G. Hill, "Investigation into the ultrasonic setting of glass ionomer cements: Part I. Postulated modalities", *Journal of Materials Science Letters*, vol. 22, pp. 539-541, 2003.

[12] A. Guida, R. G. Hill, M. R. Towler, S. Eramo, "Fluoride release of model glass ionomer cements", *Journal of Materials Science: Materials in Medicine*, vol. 13, pp.

645-649, 2002.

[13] S. G. Griffin and R. G. Hill, “Influence of glass composition on the properties of glass polyalkenoate cements. Part IV: influence of fluorine content”, *Biomaterials*, vol. 2, pp. 693–698, 2000.

[14] S. G. Griffin and R. G. Hill, “Influence of glass composition on the properties of glass polyalkenoate cements. Part I: influence of aluminium to silicon ratio”, *Biomaterials*, vol. 20, pp. 1579–1586, 1999.

[15] R. Hill, D. Wood, and M. Thomas, "Trimethylsilylation analysis of the silicate structure of fluoro-alumino-silicate glasses and the structural role of fluorine", *Journal of Materials Science*, vol. 34, pp. 1767-1774, 1999.

[16] S. G. Griffin and R. G. Hill, “Influence of glass composition on the properties of glass polyalkenoate cements. Part II: influence of phosphate content”, *Biomaterials*, vol. 21, pp. 399–403, 2000.

[17] R. G. Hill, A. Stamboulis, and R. V. Law, “Characterisation of fluorine containing glasses by F-19, Al-27, Si-29 and P-31 MAS-NMR spectroscopy”, *Journal of Dentistry*, vol. 34, pp. 525–532, 2006.

[18] E. De Barra and R. G. Hill, “Influence of glass composition on the properties of glass polyalkenoate cements. Part III: influence of fluorite content”, *Biomaterials*, vol. 21, pp. 563–569, 2000.

[19] S. G. Griffin and R. G. Hill, “Glass composition influence on glass polyalkenoate cement mechanical properties”, *Journal of Non-Crystalline Solids*, vol. 196, pp. 255-259, 1996.

[20] R. Hill and D. Wood, “Apatite-mullite glass ceramics”, *Journal of Materials Science*, vol. 6, pp. 311–318, 1995.

[21] C. M. Gorman and R. G. Hill, “Heat-pressed ionomer glass-ceramics. Part I: an investigation of flow microstructure”, *Dental Materials*, vol.19, pp. 320-326, 2003.

[22] C. Moisescu, C. Jana, S. Habelitz, G. Carl, and C. Russel, “Oriented fluoroapatite glass-ceramics”, *Journal of Non-Crystalline Solids*, vol. 248, pp. 176-182, 1999.

[23] J. C. C. Chan, R. Ohnsorge, K. Meise-Gresch, H. Eckert, W. Holand, and V. Rheinberger, “Apatite crystallization in an aluminosilicate glass matrix: Mechanistic

studies by X-ray powder diffraction, thermal analysis, and multinuclear solid-state NMR spectroscopy", *Chemistry of Materials*, vol. 13, pp. 4198-4206, 2001.

[24] A. Dias, J. Skakle, I. Gibson, J. Santos & M. Lopes (1988), "Calcium phosphate materials in restorative dentistry: a review," *Advanced Dental Research*, vol. 2, no. 1, pp. 164-180.

[25] A. Dias, M. Lopes, I. Gibson & J. Santos (2003), "In vitro degradation studies of calcium phosphate glass ceramics prepared by controlled crystallization", *Journal of Non-Crystalline Solids*, vol. 330, pp. 81-89

[26] P. Ducheyne & Q. Qiu (1999), "Bioactive ceramics: the effect of surface reactivity on bone formation and bone cell function", *Biomaterials*, vol. 20, no. 23-24, pp. 2287-2303

[27] A Dias, J Skakle, I Gibson, J Santos & M Lopes. Calcium phosphate materials in restorative dentistry: a review, *Advanced Dental Research*, vol. 2, no. 1, 1988, pp. 164-180.

[28] A. Calver, R. G. Hill, and A. Stamboulis, "Influence of fluorine content on the crystallization behavior of apatite-wollastonite glass ceramics", *Journal of Materials Science*, vol. 39, pp. 2601-2603, 2004.

[29] L. vanWullen, L. Zuchner, W. MullerWarmuth, and H. Eckert, "B-11{Al-27} and Al-27{B-11} double resonance experiments on a glassy sodium aluminoborate", *Solid State Nuclear Magnetic Resonance*, vol. 6, pp. 203-212, 1996.

[30] M. Bengisu, R. K. Brow, E. Yimaz, A. Mogus-Milankovic, and S. T. Reis, "Aluminoborate and aluminoboro silicate glasses with high chemical durability and the effect of $P_2O_5$ additions on the properties", *Journal of Non-Crystalline Solids*, vol. 352, pp. 3668-3676, 2006.

[31] H. Doweidar, Y. M. Moustafa, S. Abd El-Maksoud, and H. Silim, "Properties of $Na_2O$-$Al_2O_3$-$B_2O_3$ glasses", *Materials Science And Engineering A-Structural Materials Properties Microstructure And Processing*, vol. 3001, pp. 207-212, 2001.

[32] G. El-Damrawi and H. Doweidar, "Dependence of properties on structural units in $Li_2O$-$Al_2O_3$-$SiO_2$ glasses", *Physics And Chemistry of Glasses*, vol. 42, pp. 116-120, 2001.

[33] P. Pernice, S. Esposito, A. Aronne, and V. N. Sigaev, “Structure and crystallization behavior of glasses in the $BaO$-$B_2O_3$-$Al_2O_3$ system”, *Journal of Non-Crystalline Solids*, vol. 258, pp. 1-10, 1999.

[34] A. D. Neve, V. Piddock, and E. C. Combe, “Development of novel dental cements. I. Formulation of aluminoborate glasses”, *Clinical Materials*, vol. 9, pp. 7-12, 1992.

[35] A. D. Neve, V. Piddock, and E. C. Combe, “The effect of glass heat treatment on the properties of a novel polyalkenoate cement”, *Clinical Materials*, vol. 12, pp. 113-115, 1993.

[36] A. D. Neve, V. Piddock, and E. C. Combe, “Development of novel dental cements. II. Cement properties”, *Clinical Materials*, vol. 9, pp. 13-20, 1992.

[37] I. W. Donald, B. L. Metcalfe, D. J. Bradley, M. J. C. Hill, L, McGrath, and A. D. Bye, “The preparation And Properties Of Some Lithium Borate Based Glasses”, *Journal Of Materials Science*, vol. 29, pp. 6379-6396, 1994.

[38] S. M. Abo-Naf, F. H. El Batal, and M. A. Azooz, “Characterization of some glasses in the system $SiO_2$, $Na_2O$-RO by infrared spectroscopy”, *Materials Chemistry and physics*, vol. 77, pp. 846-852, 2003.

[39] A. D. Wilson, S. Crisp, H. J. Prosser, B. G. Lewis, and S. A. Merson, “Aluminosilicate glasses For Poly-Electrolyte Cements”, *Industrial & Engineering Chemistry Product Research And Development*, vol.19, pp. 263-270, 1980.

[40] K. Greene, M. J. Pomeroy, S. Hampshire, and R. Hill, “Effect of composition on the properties of glasses in the K2O-BaO-MgO-$SiO_2$-$Al_2O_3$-$B_2O_3$-$MgF_2$ system”, *Journal of Non-Crystalline Solids*, vol. 325, pp. 193-205, 2003.

[41] C. Moisescu, C. Jana, and C. Russel, “Crystallisation of rod-shaped fluoroapatite from glass melts in the system $SiO_2$-$Al_2O_3$-$CaO$-$P_2O_5$-$Na_2O$-$K_2O$-F”, *Journal of Non-Crystalline Solids*, vol. 248, pp. 169-175, 1999.

[42] A. Calver, R. G. Hill and A. Stamboulis, “Influence of fluorine content on the crystallization behavior of apatite-wollastonite glass-ceramics”, *Journal of Non-Crystalline Solids*, vol. 248, pp. 169-175, 1999.

[43] A. Clifford and R. Hill, “Apatite-mullite glass-ceramics”, *Journal of Materials*

*Science*, vol. 39, pp. 2601-2603, 2004.

[44] R. D. Goodridge, D. J. Wood, C. Ohtsuki, and K. W. Dalgarno, "Biological evaluation of an apatite-mullite glass-ceramic produced via selective laser sintering", *Acta Biomaterialia*, vol. 3, pp. 221-231, 2007.

[45] D. Boyd, M. R. Towler, R. V. Law, and R. G. Hill, "An investigation into the structure and reactivity of calcium-zinc-silicate ionomer glasses using MAS-NMR spectroscopy", *Journal of Materials Science: Materials in Medicine*, vol. 17, 2006.

[46] B.E. Yekta, P. Alizadeh, and L. Rezazadeh, "Synthesis of glass-ceramic glazes in the $ZnO$-$Al_2O_3$-$SiO_2$-$ZrO_2$ system", *Journal of the European Ceramic Society*, vol.27, pp. 2311-2315, 2007.

[47] G. Lusvardi, G. Malavasi, L. Menabue, and M. C. Menziani, "Synthesis, characterization, and molecular dynamics simulation of $Na_2O$-$CaO$-$SiO_2$-$ZnO$ glasses", *Journal of Physical Chemistry B*, vol. 106, pp. 9753-9760, 2002.

[48] Y.-H. Cho, S.-J. Lee, J. Y. Lee, S. W. Kim, C. B. Lee, W. Y. Lee, and M. S. Yoon, "Antibacterial effect of intraprostatic zinc injection in a rat model of chronic bacterial prostatitis", *International Journal of Antimicrobial Agents*, vol. 19, pp. 576-582, 2002.

[49] C. M. Gorman and R. G. Hill, "Heat-pressed ionomer glass-ceramics. Part II. Mechanical property evaluation", *Dental Materials*, vol. 20, pp. 252-261, 2004.

[50] Wu C, Chang J, Zhai W, "A novel hardystonite bioceramic: preparation and characteristics", *Ceram Int*, vol. 31(1), pp. 27–31, 2005.

[51] R. G. Hill, S. Kenny, B. Fennell, "The influence of poly(acrylic acid) molar mass and concentration on polyalkenoate bone cements", *In: Proceedings of the 25th Annual Meeting of the Society for Biomaterials*, USA, , pp. 1114, 2000.

[52] M. Darling, R. Hill, "Novel polyalkenoate (glass-ionomer) dental cements based on zinc silicate glasses", *Biomaterials*, vol. 15(4), pp. 299–306,1994.

[53] W. H. Zachariasen, "The atomic arrangements in glass", *Journal of the American Chemical Society*, vol. 54, pp. 3841-3851, 1932.

[54] W. Lowenstein, "The distribution of aluminium in the tetrahedral of silicates and

aluminates", *American Mineralogist*, vol. 39, pp. 92-96, 1954.

[55] J. F. Stebbins and Z. Xu, " NMR evidence for excess non-bridging oxygen in an aluminosilicate glass", *Nature*, vol. 390, pp. 60-62, 1997.

[56] C. O. Freeman, I. M. Brook, A. Johnson, P. V. Hatton, R. G. Hill, and K. T. Stanton, "Crystallization modifies osteoconductivity in an apatite-mullite glass-ceramic", *Journal of Materials Science: materials in Medicine*, vol. 14, pp. 985-990, 2003.

[57] R. Hill, A. Calver, A. Stamboulis, and N. Bubb, "Real time nucleation and crystallization studies of a fluorapatite glass-ceramics using small angle neutron scattering and neutron diffraction", *Journal of the American Ceramic Society*, vol. 90, pp. 763-768, 2007.

[58] R.Hill, A. Calver, S. Skinner, A. Stamboulis, and R. Law, "A MAS-NMR and combined Rietveldt study of mixed calcium/strontium fluorapatite glass-ceramics", in *Bioceramics 18, Pts 1 And 2, vol. 309-311, Key Engineering Materials*, pp. 305-308, 2006.

[59] A. Clifford, A. Rafferty, R. Hill, P. Mooney, D. Wood, B. Samuneva, and S. Matsuya, "The influence of calcium to phosphate ratio on the nucleation and crystallization of apatite glass-ceramics", *Journal of Materials Science: Materials in Medicine*, vol. 12, pp. 461-469, 2001.

[60] A. Stamboulis, R. G. Hill, and R. V. Law, "Characterization of the structure of calcium alumino-silicate and calcium fluoro-alumino-silicate glasses by magic angle spinning nuclear magnetic resonance (MAS-NMR)", *Journal of Non-Crystalline Solids*, vol.333, pp. 101–107, 2004.

[61] A. Stamboulis, R. G. Hill, and R. V. Law, "Structural characterization of fluorine containing glasses by F-19 Al-27 Si-29 and P-31 MAS-NMR spectroscopy", *Journal of Non-Crystalline Solids*, vol. 351, pp. 3289-3295, 2005.

[62] A. Stamboulis, R. G. Hill, R. V. Law, and S. Matsuya, "MAS-NMR study on the crystallization process of apatite-mullite glass ceramics", *Physics and Chemistry of Glasses*, vol. 45, pp. 127-133, 2004.

[63] R. J. Kirkpatrick and R. K. Brow, "Nuclear-Magnetic-Resonance investigation of

the structures of phosphate and phosphate-containing glasses- a review", *Solid State Nuclear magnetic Resonance*, vol. 5, pp. 9-21, 1995.

[64] R. Dupree, D. Holland, M. G. Mortuza, J. A. Collins, and M. W. G. Lockyer, "Magic angle spinning NMR of alkali phosphor-aluminosilicate glasses", *Journal of Non-Crystalline Solids*, vol. 112, pp. 111-119, 1989.

[65] B. E. Kent, B. G. Lewis, and A. D. Wilson, "Glass ionomer cement formulations. 1. Preparation of novel fluoroaluminosilicate glasses high in fluorine", *Journal of Dental Research*, vol. 58, pp. 1607-1619, 1979.

[66] T. J. Kiczenski, L.-S. Du, and J. F. Stebbins, "F-19 NMR study of the ordering of high field strength cations at fluoride sites in silicate and aluminosilicate glasses", *Journal of Non-Crystalline Solids*, vol. 337, pp. 142-149, 2004.

[67] R. G. Hill and A. D. Wilson, "Some structural aspects of glasses used in ionomer cements", *Glass Technology*, vol. 29, pp. 150-157, 1988.

[68] Q. Zeng and J. F. Stebbins, "Fluoride sites in aluminosilicate glasses: High-resolution F-19 NMR results", *American Mineralogist*, vol. 85, pp. 863-867, 2000.

[69] J. F. Stebbins, S. Kroeker, S. K. Lee, and T. J. Kiczenski, "Quantification of five- and six-coordinated aluminum ions in aluminosilicate and fluoride-containing glasses by high-field, high-resolution Al-27 NMR", *Journal of Non-Crystalline Solids*, vol. 275, pp. 1-6, 2000.

[70] S. Jalota, S. B. Bhaduri, and A. C. Tas, " A new rhenanite (beta-NaCaPO4) and hydroxyapatite biophasic biomaterial for skeletal repair", *Journal of Biomedical Materials Research Part B-Applied Biomaterials*, vol. 80B, pp. 304-316, 2007.

[71] T. Nakamura, T. Yamamuro, S. Higashi, T. Kokubo, and S. Itoo, "A New Glass-Ceramic For Bone-Replacement- Evaluation Of Its Bonding To Bone Tissue", *Journal of Biomedical Materials research*, vol. 19, pp. 685-698, 1985.

[72] P. J. Adair and D. G. grossman, "The castable ceramic crown", *Int J Periodontics Restorative Den*t, vol. 4, pp. 32-46, 1984.

[73] A. Rafferty, A. Clifford, R. Hill, D. Wood, B. Samuneva, and M. DimitrovaLukacs, "Influence of fluorine content in apatite-mullite glass ceramics",

*Journal of the American Ceramic Society*, vol. 83, pp. 2833-2838, 2000.

[74] L. L. Burgner and M. C. Weinberg, "Crystal growth mechanisms in inorganic glasse", *Physics and Chemistry of Glasses*, vol. 42, pp. 184-190, 2001.

[75] A. K. Varshneya, *Fundamentals of inorganic glasses*: Society of Glass Technology, 2006.

[76] W. Hoeland, V. Rheinberger, and M. Frank, "Mechanisms of nucleation and controlled crystallization of needle-like apatite in glass-ceramics of the $SiO_2$-$Al_2O_3$-$K_2O$-CaO-$P_2O_5$ system", *Journal of Non-Crystalline Solids*, vol. 253, pp. 170-177, 1999.

[77] J. W. Cahn and R. J. Charles, "Initial Stages Of Phase Separation In Glasses", *Physics And Chemistry Of Glasses*, vol. 6, pp. 181-191, 1965.

[78] P. Griffiths, de J. A. Hasseth, "Fourier Transform Infrared Spectrometry (2nd ed.)", Wiley-Blackwell. ISBN 0471194042, 2007.

[79] C. N. Banwell, E. M. McCash, "Fundamentals of Molecular Spectroscopy (4th ed.)", McGraw-Hill. ISBN 0-07-707976-0, 1994.

[80] D. J. Gardiner, "Practical Raman spectroscopy", Springer-Verlag. ISBN 978-0387502540, 1989.

[81] L. Stoch and M. Sroda, "Infrared spectroscopy in the investigation of oxide glasses structure", *Journal of Molecular Structure*, vol. 512. Pp. 77-84, 1999.

[82] N.J. Clayden, S. Esposito, A. Aronne, and P. Pernice, "Solid state Al-27 NMR and FTIR study of lanthanum aluminosilicate glasses", *Journal of Non-Crystalline Solids*, vol. 258, pp.11-19, 1999.

[83] S. A. MacDonald, C. R. Schardt, D. J. Masiello, and J. H. Simmons, "Dispersion analysis of FTIR reflection measurements in silicate glasses", *Journal of Non-Crystalline Solids*, vol. 275, pp. 72-82, 2000.

[84] C. Huang and E. C. Behrman, "Structure And Properties Of Calcium Aluminosilicate Glasses", *Journal of Non-Crystalline Solids*, vol. 128, pp. 310-321, 1991.

[85] L.G. Hwa, S. L. Hwang, and L. C. Liu, "Infrared and Raman spectra of calcium-alumino-silicate glasses", *Journal of Non-Crystalline Solids*, vol. 238, pp.

193-197, 1998.

[86] N. Shibata, M. Horiguchi and T. Edahiro, *Journal of Non-Crystalline Solids*, 45, 115, 1981.

[87] R. Shuker and R. W. Gammon, *Physics. Rev. Lett*. 25, 222, 1970.

[88] R. Shuker and R.W. Gammon, *Journal of Physics And Chemistry of Solids*, 25, 222, 1970.

[89] J. Etchepare, in Amorphous Materials, eds. R. W. Douglas and B. Ellis, pp. 337,1970.

[90] P.L. Higby, R.J. Ginther, I.D. Aggarwal, E.J. Friebele, *Journal of Non-Crystalline Solids*, 126, 209, 1990.

[91] MacMillan, B. Piriou, *Journal of Non-Crystalline Solids*, 55 221, 1983.

[92] C. Huang, E.C. Behrman, *Journal of Non-Crystalline Solids*, 128, 310, 1991.

[93] C.I. Merzbacher, W.B. White, *Journal of Non-Crystalline Solids*, 130 18, 1991.

[94] P. Colomban, H. G. M. Edwards & J. M. Chalmers, "Recognition of ancient technology from the Raman spectra", pp. 192–206, 2000.

[95] Jayaraman A., Wood D. L. & Maines R. G, "High pressure Raman study of the vibrational modes in AlPO4 and SiO2 (α-quartz)", *Physics*. B 35:8316–8321, 1987.

[96] X. ChengLi, "Study on Synthesis and Preparation of Corundum /Mullite /Gahnite-based Multiphase Materials", 2003.

[97] Eleni Maria Kartelia, MRes thesis 2010，University of Birmingham。

[98] University of Birmingham and Fei Wang, PHD thesis 2009, University of Birmingham.

[99] S. W. Kieffer (1979), Rev. Geophys. *Space Phyics*. 17, 20.

[100] R. N. Panda, M. F. Hsieh, R. J. Chung, and T. S. Chin, "FTIR, XRD, SEM and solid state NMR investigations of carbonate-containing hydroxyapatite nanoparticles synthesized by hydroxide-gel technique", *Journal of Physics And Chemistry of Solids*, vol. 64, pp. 193-199, 2003.

[101] S.Haque, I. Rehman, and J. A. Darr, "Synthesis and characterization of grafted nanohydroxyapatites using functionalized surface agents" , *Langmuir*, vol. 23, pp.

6671-6676, 2007.

[102] Adak AK, A. Pathak, P. Pramanik and J Mater, *Science Lett*, vol. 17, pp. 559, 1998.

[103] L. Kravitz, J.Kingsley, E. Elkin, *Journal of Chemical Physics.* 49. 4600, 1968.

[104] A. Schulte, S. Buchler, B. Chai, Proc. Soc. Photo-Opt. Instrument. Engeering. 2380, 34, 1995.

[105] W. Griffith, *Nature* (Landon) 224, 264, 1969.

[106] M. Sha, Z. Li, R. Bradt, *Journal of Applied Physics,* 75 7784, 1994.

[107] G. Herzberg, Infrared and Raman Spectra, Van Nostrand, New York, 1945.